

12-2021

Detrital Zircon U-Pb Geochronology of Upper Mississippian Siltstone, Oklahoma and Arkansas

Linnea Johnson
University of Arkansas, Fayetteville

Follow this and additional works at: <https://scholarworks.uark.edu/etd>



Part of the [Geology Commons](#), and the [Stratigraphy Commons](#)

Citation

Johnson, L. (2021). Detrital Zircon U-Pb Geochronology of Upper Mississippian Siltstone, Oklahoma and Arkansas. *Graduate Theses and Dissertations* Retrieved from <https://scholarworks.uark.edu/etd/4311>

This Thesis is brought to you for free and open access by ScholarWorks@UARK. It has been accepted for inclusion in Graduate Theses and Dissertations by an authorized administrator of ScholarWorks@UARK. For more information, please contact scholar@uark.edu, uarepos@uark.edu.

Detrital Zircon U-Pb Geochronology of Upper Mississippian Siltstone, Oklahoma and Arkansas

A thesis submitted in partial fulfillment
of the requirements for the degree of
Master of Science in Geology

by

Linnea L. Johnson
Illinois State University
Bachelor of Science in Geology, 2019

December 2021
University of Arkansas

This thesis is approved for recommendation to the Graduate Council.

Glenn Sharman, Ph.D.
Thesis Advisor

Gregory Dumond, Ph.D.
Committee Member

Walter Manger, Ph.D.
Committee Member

Barry Shaulis, Ph.D.
Committee Member

Abstract

Although Upper Mississippian strata have been characterized extensively using lithostratigraphy, sequence stratigraphy, and biostratigraphy across the North American midcontinent, the origin of the silt comprising the Meramec STACK (Sooner Trend Anadarko Basin, Canadian and Kingfisher counties) reservoirs of the Anadarko Basin in west-central Oklahoma and age equivalent units is not well understood, despite its economic importance as an unconventional petroleum reservoir. Previously published models have variously invoked fluvial, marine, and aeolian sediment transport for Upper Mississippian siltstone present along the paleo-shelf edge of the Laurentian craton.

This study uses detrital zircon U-Pb geochronology and grain morphology, handheld x-ray fluorescence (hXRF) whole rock geochemistry, and petrography to constrain sediment provenance of Upper Mississippian (Meramecian and Chesterian) strata along the Laurentian paleo-shelf edge. Conservative mineral separation techniques were developed to facilitate processing of silt-sized material, allowing efficient recovery in small (i.e., <100 g) samples.

Detrital zircon U-Pb age and grain morphology data reported in this study indicate that Upper Mississippian silt-sized detritus was not only sourced from Laurentia but was also sourced from advancing peri-Gondwanan terranes to the south and/or east. Of the 2478 detrital zircon analyses measured from nineteen Meramecian siltstone samples, 32% were Grenville (900-1350 Ma), 21% were Appalachian (240-500 Ma), and 17% were peri-Gondwanan (500-900 Ma).

Zircon grain size and morphology data complements U-Pb age data and provides additional insight into potential sediment transport mechanisms of the Meramecian silt. Peri-Gondwanan detrital zircons (500-900 Ma) are smaller and more spherical than Appalachian

(240-500 Ma) or Grenville (900-1300 Ma) zircon, suggesting that these peri-Gondwanan grains may have traveled greater distances. Age-equivalent samples on the craton of Laurentia do not possess a significant component of 500-900 Ma zircon, suggesting peri-Gondwana grains along the paleo-shelf edge were transported via marine currents rather than by wind. The combination of detrital zircon U-Pb ages, morphology data, and petrographic observations support a model for long-distance transport of peri-Gondwanan zircon to the southern Laurentian margin via contour-parallel marine currents. These far travelled grains mixed with detritus sourced from the easterly Appalachian Orogeny along the southern paleo-shelf edge of Laurentia. This study documents a significant peri-Gondwanan influence in the southern midcontinent of North America during Meramecian time, the presence of which predates the consequent arrival of these southerly terranes during the collision of southern Laurentia with Gondwana.

©2021 by Linnea L. Johnson
All Rights Reserved

Acknowledgements

This study is funded by Devon Energy and the Detrital Geochronology Laboratory (including California Resources Corporation and Chevron Corporation). Funding helped to cover costs of thin section preparation and laboratory work conducted at the University of Arkansas Trace Element and Radiogenic Isotope Laboratory (TRAIL).

Thanks to Dave Hull, Will Cains, and others from Devon Energy for their help, including allowing access to core samples, supplying detailed core imagery, and providing invaluable insights to expand this study. Thanks to Andrew Cullen for collecting samples from the Ardmore Basin and taking the time to help progress my research in a multitude of ways.

Thanks to David Gates, Greg Dumond, and Mac McGilvery for their collective help in advancing my research on and off-campus. Thanks to Barry Shaulis for giving his time to help run samples in the laser lab and providing support on my committee. A special thanks to Walt Manger for serving as a committee member, and for sharing his vast knowledge and expertise in the field.

Many thanks to Glenn Sharman for being a remarkable graduate advisor and mentor. His incredible work ethic, continual desire to learn, and passion for geology have molded me to become a better geologist and researcher.

Dedication

This thesis is dedicated to my family and loved ones, who instilled in me the value of integrity and hard work. Thank you for being a constant support in all my endeavors.

Table of Contents

Chapter 1: Introduction.....	1
1.1 Introduction.....	1
Chapter 2: Geologic Background.....	4
2.1 Mississippian Paleogeography, Tectonics, and Basin Formation.....	4
2.2 Mississippian Climate and Lithologic Characteristics.....	7
2.3 Oklahoma STACK.....	8
2.4 Previous Interpretations of Upper Mississippian Silt Provenance.....	9
Chapter 3: Methods.....	11
3.1 Sampling.....	11
3.2 Petrographic Analysis.....	13
3.3 hXRF Analysis.....	14
3.4 Mineral Separation.....	15
3.5 High Resolution Grain Imaging.....	16
3.6 Detrital Zircon U-Pb Geochronology.....	17
3.7 Detrital Zircon Morphology.....	18
Chapter 4: Results.....	20
4.1 Petrographic Analysis.....	20
4.2 hXRF Analysis.....	21
4.3 Detrital Zircon U-Pb Geochronology.....	24
4.3.1 Anadarko Basin (Canadian and Dewey Counties).....	27
4.3.2 Ardmore Basin (Sycamore and Caney).....	29
4.3.3 Arkoma Shelf (Pryor Creek).....	29
4.3.4 Arkoma Shelf (Moorefield and Batesville).....	30
4.4 Zircon Morphological Analysis.....	31
Chapter 5: Discussion.....	32
5.1 Provenance of Meramecian Silt.....	32

5.2 Sedimentary Transport Pathways	35
Chapter 6: Conclusions.....	39
6.1 Conclusions.....	39
References.....	41
Appendix.....	50
Table 1	50
Table 2	52
Table 3	55

Chapter 1: Introduction

1.1 Introduction

Explanations of sediment transport and provenance for Upper Mississippian to Pennsylvanian detritus along the southern edge of Laurentia have included contrasting interpretations of fluvial, marine, and aeolian mechanisms (Fig. 1; Gehrels et al., 2011; Xie et al.,

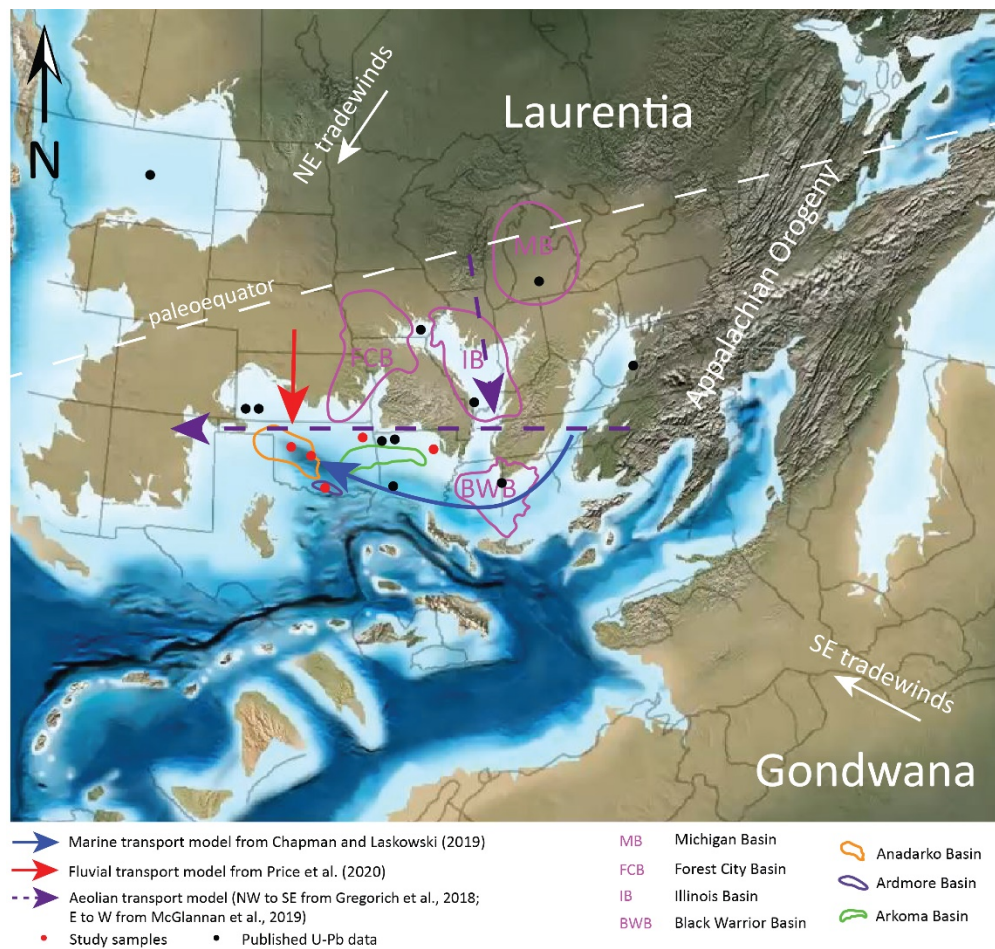


Figure 1. Paleogeographic reconstruction of North America (Laurentia) during Late Mississippian time (~320 Ma). Displayed are the three competing sediment transport models, including fluvial (Price et al., 2020), marine (Chapman and Laskowski, 2019), and aeolian (Gregorich et al., 2018; McGlannan et al., 2019). Modified from Blakey, 2020.

2016a; Xie et al., 2016b; Thomas et al., 2017; Xie et al., 2018; Chapman and Laskowski, 2019;

McGlannan et al., 2019; Wang and Bidgoli, 2019; Price et al., 2020; Thomas et al., 2020;

Lawton et al., 2021; Thomas et al., 2021). Upper Mississippian deposits of Osagean, Meramecian, and Chesterian age comprise the STACK (Sooner Trend Anadarko Basin, Canadian and Kingfisher counties) play of the Anadarko Basin, west-central Oklahoma, which has grown to be an important unconventional resource play in the United States (Fig. 2; Wittman, 2013; Price et al., 2017; Price et al., 2020). The Meramecian interval in the STACK play and age-equivalent strata across the North American midcontinent are dominantly siliciclastic siltstones to very-fine sandstones, with varying degrees of carbonate and clay content (Shelley, 2016; Miller, 2018; Cullen, 2019; Gates, 2020; Price et al., 2020). Identifying the source(s) and transport pathway(s) of sediment forming the Upper Mississippian Meramec Series would expand current understanding of the Anadarko Basin’s evolution and provide valuable insights relating to the origin of silty unconventional reservoirs in the STACK play.

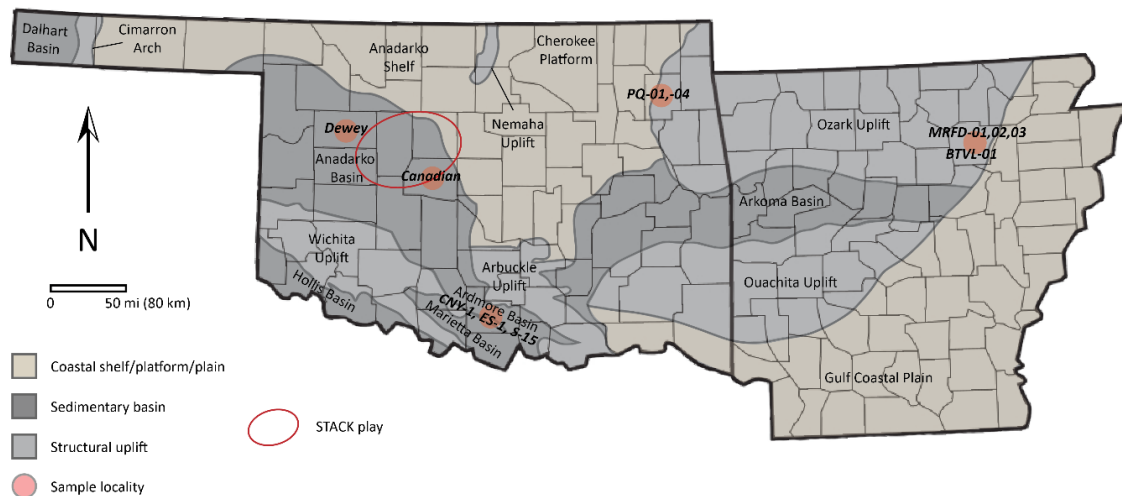


Figure 2. Geologic provinces of Oklahoma and Arkansas, showing the location of samples presented in this study. Modified from Northcutt and Campbell, 1995; and Nance, 2018.

The Meramec reservoir is the highest producing unconventional interval of the STACK play (Wittman, 2013). Cumulative hydrocarbon production from the Anadarko Basin has been roughly 50 billion barrels of oil equivalent (BOE) with an estimated 50 billion BOE of additional potential remaining for future production from unconventional reservoirs (Fritz and Mitchell,

2021). Continued advancements in drilling and completion techniques of unconventional reservoirs within the past decade have fueled interest in hydrocarbon production from the Meramec Series in the Anadarko Basin (Hardwick, 2018).

Age (Ma)	System	Series	Stage	ANADARKO BASIN, W OKLAHOMA	ARDMORE BASIN, S OKLAHOMA	ARKOMA BASIN, NE OKLAHOMA	EASTERN ARKANSAS			
316	PENNSYLVANIAN	Lower Pennsylvanian	Atokan	Thirteen Finger Lime	Dornick Hills Group	Atoka Formation	Hale Formation			
			Morrowan	Morrow Group		Morrow Shale		Wapanucka McCully		
				Morrow Group		Purdy Sand		Union Valley Sausbee		
						Puryear Sand				
323			Springer Formation	Springer Formation						
336	MISSISSIPPIAN	Upper Mississippian	Chesterian	Chester Group	Manning Zone	Pitkin Limestone	Pitkin Formation			
						Fayetteville Shale	Fayetteville Shale			
			Meramecian	Meramec Lime	Meramec Lime	Sycamore Limestone	Caney Shale	Hindsville Formation	Hindsville Limestone	
							Ste. Genevieve Limestone	Pryor Creek Formation	Ordnance Plant Mbr	Ruddell Shale
							St. Louis Limestone		Lindsey Bridge Mbr	Moorefield Formation
							Salem Limestone		Bayou Manard Mbr	
Warsaw Limestone										
345	Lower Mississippian	Osagean	Osage Lime	Mississippi Chat	Boone Group	Boone Group				
				Cowley Formation	St. Joe Group	St. Joe Group				
				Mississippi Solid						

Figure 3. Upper Mississippian and Lower Pennsylvanian stratigraphic intervals sampled across Oklahoma and Arkansas. Sampled intervals are shown as red polygons. Modified after Johnson and Cardott, 1992; Romera and Philp, 2012; Higley, 2013; Lohr et al., 2013; Xie et al., 2016a; Cullen, 2019.

To better understand the sediment routing and provenance of Upper Mississippian silt along the southern margin of Laurentia in Arkansas and Oklahoma, a multi-proxy provenance assessment involving detrital zircon U-Pb geochronology and grain morphology, hXRF whole rock geochemistry, and petrographic analysis was conducted. A total of 19 new detrital zircon U-Pb samples (2478 U-Pb analyses) are reported herein and juxtaposed with compilations of

previously published detrital zircon data from Upper Mississippian to Pennsylvanian strata across the North American Craton (Park et al, 2010; Xie et al., 2016a; Xie et al., 2016b; McGuire, 2017; Thomas et al., 2017; Xie et al., 2018; Chapman and Laskowski, 2019; Wang and Bidgoli, 2019; Thomas et al., 2020; Thomas et al., 2021). Detrital zircon U-Pb ages paired with grain morphology and geochemistry were utilized to test models for sediment sources and transport pathways to the Anadarko Basin (Meramec Series) via comparison with age-equivalent units in the Ardmore and Arkoma basins and across the North American Craton (Fig. 3).

Chapter 2: Geologic Background

2.1 Mississippian Paleogeography, Tectonics, and Basin Formation

The Late Mississippian time interval (roughly 331-323 Ma) is marked by major shifts in global climate, tectonics, and atmospheric and oceanic circulation (Wang and Bidgoli, 2019; Lawton et al., 2021; Thomas et al., 2021). North American sediment sources from the Mississippian Period to the Permian Period were primarily controlled by the evolving Alleghanian-Ouachita-Sonora (AOMS) orogen, initiated by the collision of Laurentia and Gondwana (Dickinson and Gehrels, 2003; Poole et al., 2005; Gehrels et al., 2011; Thomas, 2011; Leary et al., 2020; Lawton et al., 2021). Several lithospheric tracts designated as peri-Gondwanan terranes were located between the colliding continents (Dickinson and Gehrels, 2003; Lawton et al., 2021). Peri-Gondwanan crustal provinces, including the Sabine Terrane, the Suwannee Terrane, and the North Gondwana Arc, formed as magmatic arcs (e.g., Carolina Terrane) or via accretionary orogenesis along Gondwana's active margin (e.g., Avalon, Carolina,

and Suwannee terranes) (Fig. 4; Wortman et al., 2000; Dickinson and Lawton, 2001; Dickinson and Gehrels, 2003; Lawton et al., 2021).

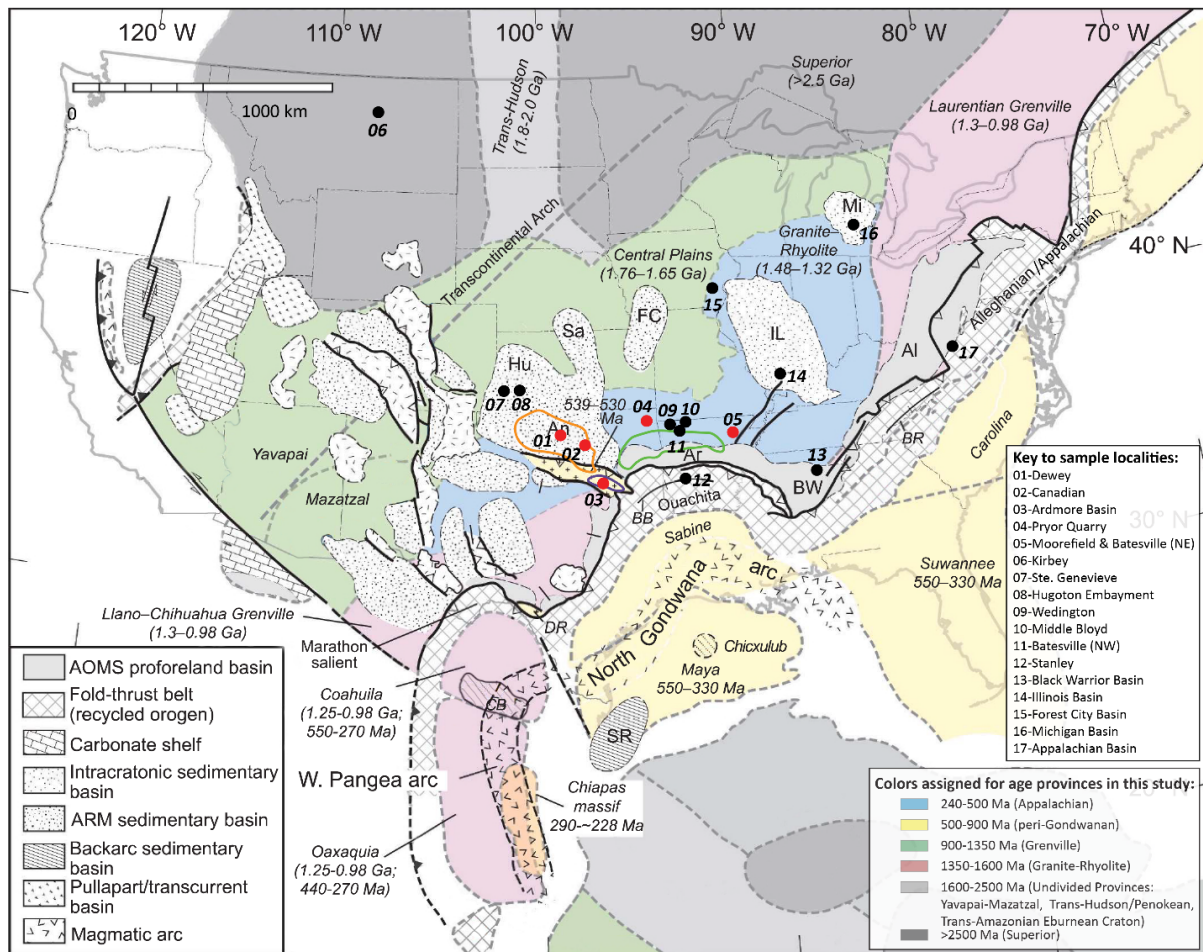


Figure 4. Geologic provinces of North America, highlighting Upper Mississippian sample locations from this study (red circles) and published data (black circles). Note the peri-Gondwanan terranes are shown in yellow and the Appalachian orogen is also referred to as the Alleghanian. Modified from Lawton et al., 2021.

Additional peri-Gondwanan terranes (i.e., Maya Block, Oaxaquia Terrane, Coahuila Terrane, Gondwanan arcs) were also present during Paleozoic time (Fig. 4; Lopez et al., 2001; Alemán-Gallardo et al., 2019; Snedden and Galloway, 2019; Lawton et al., 2021). The Maya Block (550-330 Ma), located on the south side of the Gulf of Mexico, was emplaced in Neoproterozoic crust, but has been largely covered by a Paleogene-Neogene carbonate succession (Fig. 4; Pindell and Kennan, 2009; Snedden and Galloway, 2019; Lawton et al.,

2021). The Oaxaquia Terrane (1.25-0.98 Ga; 440-270 Ma), forms the majority of eastern Mexico, consisting of Grenville granite, metagranite, and locally intruded metamorphic rocks (Fig. 4; Ortega-Gutiérrez et al., 1995; Lawlor et al., 1999; Alemán-Gallardo et al., 2019; Lawton et al., 2021). The Coahuila Terrane (1.25-0.98 Ga; 550-270 Ma), north of the Oaxaquia Terrane, contains Carboniferous volcanic rocks and a thick succession of turbidites and volcanic and carbonate olistoliths (Fig. 4; Ortega-Gutiérrez et al., 1995; McKee et al., 1999; Lawton et al., 2021).

During the early Paleozoic, crustal blocks were transferred between Laurentia and Gondwana (Keppie et al., 1996; Thomas and Astini, 1996; Lawton et al., 2021). Collision of Gondwana with the southeastern margin of Laurentia generated the Appalachian Orogeny (also designated the Alleghanian Orogeny) driving transport of clastic sediments into the interior of the North American craton (i.e., Laurentia) (Fig. 4; Chapman and Laskowski, 2019; Wang and Bidgoli, 2019; Price et al., 2020; Thomas et al., 2020; Lawton et al., 2021; Thomas et al., 2021). The Appalachian Orogeny is a composite orogeny, consisting of the Taconic (Ordovician), Acadian (Devonian-Early Mississippian), and Alleghanian (Late Mississippian-earliest middle Permian) orogenies respectively (Hatcher Jr. et al., 1989; Becker et al., 2005, 2006; Thomas et al., 2017; Lawton et al., 2021).

Continued tectonic collision caused the Appalachian uplift to extend southwestward as the Ouachita Mountains (Ouachita Orogeny) and drove the development of several sedimentary basins (e.g., Anadarko, Ardmore, and Arkoma basins) west of the Appalachian forebulge (Fig. 4; Gutschick and Sandberg, 1983; Frazier and Schwimmer, 1987; Thomas and Astini, 1996; Manger, 2014; Wang and Bidgoli, 2019; Lawton et al., 2021). The Anadarko, Ardmore, and Arkoma basins in southern Laurentia evolved from shallow-water to deep-water deposition

during orogenesis (Gutschick and Sandberg, 1983; Miller, 2018; Price et al., 2020). Final stages of continental collision resulted in the ultimate formation of Pangea in Permian time (Manger, 2014; Wang and Bidgoli, 2019; Price et al., 2020; Lawton et al., 2021).

2.2 Mississippian Climate and Lithologic Characteristics

During the Mississippian period, global climate conditions were evolving from greenhouse conditions to icehouse conditions which continued into the Permian period (Shelley, 2016). Throughout Meramecian time, widespread shallow epicontinental seas covered the interior of North America, driving the production of a vast carbonate platform (McFarland and Bush, 2004; Chapman and Laskowski, 2019; Wang and Bidgoli, 2019; Price et al., 2020; Lawton et al., 2021). Sea level regression during Late Meramecian time caused the carbonate platform to become largely exposed and actively incised via fluvial processes (Wang and Bidgoli, 2019). The Mississippian-Pennsylvanian transition was marked by an abrupt drop in sea level, causing a shift in depositional environments from marine-dominated to fluvial-dominated (Gutschick and Sandberg, 1983; Frazier and Schwimmer, 1987; Chapman and Laskowski, 2019).

Upper Mississippian lithofacies across Laurentia include variably calcareous and argillaceous limestone, sandstone, siltstone, mudstone, and shale that record relative changes in sea level (McFarland and Bush, 2004; Miller, 2018; Cullen, 2019). Mississippian strata across northern and southern Oklahoma reflect a changing depositional environment, from the shallow-water Meramec Lime carbonate deposits in northern Oklahoma to the deep-water mixed siliciclastic-carbonate deposits in southern Oklahoma (Miller, 2018). Meramec siltstones contain variable amounts of calcareous skeletal fragments, coated grains (e.g., ooids), and peloids, and display sedimentary features including cross-stratification (e.g., flaser, wavy, lenticular,

hummocky stratification), bioturbation, and graded bedding typical of turbidite successions (Shelley, 2016; Hardwick, 2018; Miller, 2018; Gates, 2020; Price et al., 2020).

2.3 Oklahoma STACK

The STACK play is located in the midcontinent region of North America, in central-northwestern Oklahoma (Fig. 2; Price et al., 2020). The core of the STACK play is centralized in Oklahoma's Canadian, Kingfisher, and Blain counties, while the extremity of the play is present in Oklahoma's Dewey, Blaine, Woodward, and Major counties (Hardwick, 2018; Price et al., 2020). Situated south of the paleoequator, the Meramecian STACK play formed on a distally steepened ramp, with a proximal shallow-water environment to the north and deepening basinward to the south (Price et al., 2020). The Meramec Series in the STACK play is generally composed of quartz silt to very fine sand with variable proportions of carbonate and clay (Hardwick, 2018; Hickman, 2018; Miller et al., 2018; Gates, 2020; Price et al., 2020). Coarse-grained sediments were deposited proximally in the basin, whereas fine-grained sediments were deposited distally (Price et al., 2020). Calcareous facies are more prominent up-dip in the basin and argillaceous facies are more prominent basinward (Price et al., 2020).

Sedimentary features in the Meramec Formation include stacked turbidites, laminations in argillaceous facies, and hummocky to swaley cross-bedding present in the coarser siltstone and sandstone facies (Price et al., 2020). Prograding low-angle clinoforms ($<1^\circ$) stepping basinward to the southeast have been well documented in the Meramec Formation, particularly in the STACK play (Cullen, 2017; Price et al., 2017; Miller, 2018; Price et al., 2020). Price et al. (2017) and Miller (2018) have postulated the STACK clinoforms were formed in a subaqueous delta setting just below storm wave base. Rebesco et al. (2014) and Patruno and Helland-Hansen

(2018) cite instances of stacked, low-angle, prograding clinoform structures forming via contour-parallel currents.

2.4 Previous Interpretations of Upper Mississippian Silt Provenance

Studies focusing on Upper Mississippian strata within the U.S. midcontinent have increased in recent years, perhaps in part as a consequence of interest in hydrocarbon production from unconventional reservoirs (Godwin, 2017). Previous studies have sought to characterize the age, depositional setting, transport medium, rock geochemistry, and reservoir properties of Upper Mississippian sediments across the midcontinent region (Park et al., 2010; Shelley, 2016; Xie et al., 2016a; Xie et al., 2016b; Cullen, 2017; Godwin, 2017; McGuire, 2017; Thomas et al., 2017; Gregorich et al., 2018; Xie et al., 2018; Chapman and Laskowski, 2019; Cullen et al., 2019; McGlannan et al., 2019; Wang and Bidgoli, 2019; Leary et al., 2020; Price et al., 2020; Thomas et al., 2020; Lawton et al., 2021; Thomas et al., 2021).

Detrital zircon studies assessing Upper Mississippian to Pennsylvanian strata have proposed variable modes of transport and provenance for detritus along the southern edge of the North American continent (Thomas et al., 2021). Interpretations of sediment dispersal of Upper Mississippian detritus include fluvial, marine, and aeolian transport (Fig. 1; Cullen, 2017; Gregorich et al., 2018; Chapman and Laskowski, 2019; Cullen et al., 2019; McGlannan et al., 2019; Wang and Bidgoli, 2019; Price et al., 2020; Thomas et al., 2020; Lawton et al., 2021; Thomas et al., 2021).

At present, fluvial processes are the most widely accepted model for sediment transport of Upper Mississippian silt to the Laurentian paleo-shelf edge (Fig. 1; Wang and Bidgoli, 2019; Price et al., 2020). Price et al. (2020) specifically inferred a river flowing from the northeast to

the southwest as the primary transport mechanism for sediment of the STACK play, in part on the basis of low-angle ($<1^\circ$) clinoforms that prograde to the southeast, interpreted to be part of a subaqueous delta sourced by fluvial input from the north.

Wang and Bidgoli (2019) also invoked a fluvial model for sediment transport from Chesterian sandstones in southwestern Kansas and northwestern Arkansas, proposing a large, transcontinental river system with headwaters in the north and flowing southward across the midcontinent. Laminations, trough-cross beds, and carbonized organic material in the Chesterian core sample Mary Jones #2 from the Hugoton Embayment in southwest Kansas are cited as evidence of a fluvial origin (Wang and Bidgoli, 2019). Sea level regression in latest Meramecian time led to widespread subaerial exposure causing the carbonate platform to be subjected to fluvial incision and valley formation (Wang and Bidgoli, 2019). A transgression during Chesterian time resulted in valleys being filled with fine- to very fine-grained sandstones, deposits that are interpreted to reflect fluvial sedimentation from the north with a marine influence from the south (Wang and Bidgoli, 2019).

Chapman and Laskowski (2019) and Cullen et al. (2019) proposed that shallow marine processes (e.g., marine currents, tides, storms) dominated transcontinental sediment dispersal during Late Mississippian time. Chapman and Laskowski (2019) identified several potential obstacles that would impede sediment transport to the west via rivers, including sedimentary basins (the Illinois, Michigan, and Appalachian basins), paleogeographic highs (e.g., the Transcontinental Arch), and inland seas (Appalachian and Kaskaskia seas). These potential barriers to fluvial transport led Chapman and Laskowski (2019) to invoke a marine dominated sediment transport model with detritus transported from east to west via contour-parallel currents (Fig. 1).

Gregorich et al. (2018) proposed an alternative mode for silt transport in the Illinois Basin, suggesting that the Borden Silt (Kinderhookian) contained a significant proportion of ~1460 Ma zircons that were sourced from the northwest (Wolf River Batholith) and transported via aeolian processes (e.g., haboobs, monsoons) (Fig. 1). Leary et al. (2020) inferred a north to south, longshore and aeolian sediment transport system along the southwestern margin of Laurentia. Evans and Soreghan (2015) suggested that a large fraction of the eolian silt comprising the Molas Formation (Morrowan) in the Paradox Basin (Colorado) was transported from local and long-distance sources (>2000 km) in northeastern Laurentia. McGlannan et al. (2019) inferred the silts comprising the Woodford Shale, Sycamore Formation, and the lower Caney Shale (Devonian-Mississippian) were largely transported via eolian processes, blown from east to west across the Laurentian craton.

Chapter 3: Methods

3.1 Sampling

Field work was conducted during multiple excursions in 2019 and 2020. Nineteen samples from four field localities were collected across Oklahoma and eastern Arkansas, including the Anadarko Basin, Ardmore Basin, and other localities along the southern paleo-shelf of Laurentia (Table 1; Figs. 1 and 2). Approximately 0.5-1 kg of sample was collected from a restricted stratigraphic interval for each sample (Fig. 3)

Two vertical, un-oriented cores from the Meramec Series in the STACK play of the Anadarko Basin, one from Canadian County and one from Dewey County, were made available for sampling by Devon Energy (Figs. 2 and 3). Sample locations were chosen from intervals with higher Si and Zr content using hXRF data (Gates, 2020), to maximize potential for zircon yield.

Five samples (Canadian-1 through -5) were procured from the Canadian County core, which consists of thicker, more distal Meramec deposits of the STACK play (Figs. 2 and 3). Five samples (Dewey-1 through -5) were collected from the Dewey core, which encountered the thinner, more proximal Meramec deposits of the STACK play (Figs. 2 and 3).

Two samples (ES-1 and S-15) from the upper Sycamore Limestone and one sample (CNY-1) from the Caney Shale were collected by Andrew Cullen from an outcrop along I-35 in the Ardmore Basin, south-central Oklahoma (Fig. 3; Miller and Cullen, 2018; Cullen, 2019). The upper Sycamore Limestone is Meramecian in age and the Caney Shale is Chesterian in age (Fig. 3; Miller and Cullen, 2018).

Two samples (PQ-01 and PQ-04) were acquired from a strike-oriented exposure of the Meramecian Pryor Creek Formation in the southwest pit at Kemp Quarries, Inc. – Pryor Stone, Inc. in northeast Oklahoma (Fig. 2; Shelley, 2016; Gates, 2020). Detailed lithostratigraphic and sequence stratigraphic assessments of these Mississippian-Pennsylvanian strata have previously been conducted by Godwin (2010), Shelley (2016), and Gates (2020). PQ-01 was collected from the Lindsey Bridge Member of the Pryor Creek Formation and PQ-04 was collected from the Ordinance Plant Member (Fig. 3; Godwin, 2010; Shelley, 2016; Gates, 2020).

Three samples were obtained from a resistive roadcut exposure of the Meramecian Moorefield Formation (MRFD-01 through -03) just east of Moorefield, Arkansas along Highway 69 (Figs. 2 and 3). One additional sample was collected from the Chesterian Batesville Sandstone (BTVL-01), taken from an outcrop exposed south of Batesville, Arkansas along Dennison Heights (Figs. 2 and 3). Warner (2019) characterized both the Moorefield Formation and Batesville Sandstone in detail, within the same type locality. Samples from the Moorefield

Formation and Batesville Sandstone are interpreted to represent the paleo-shelf edge in northeastern Arkansas (Fig. 1).

3.2 Petrographic Analysis

Although an initial description of rocks at a macroscopic level can be conducted in the field, a higher degree of petrographic detail can be accomplished via microscopic analysis. Optical and morphological properties can be observed using a petrographic microscope, including, but not limited to, color, pleochroism, twinning, cleavage, grain form, and grain orientation (Raith et al., 2011). Samples can be impregnated with stains and dyes to assist in mineral identification and porosity, respectively (Raith et al., 2011).

Nineteen thin section billets were prepared at the University of Arkansas before being shipped to Spectrum Petrographics to be made into thin sections. Half of each thin section was stained; calcareous samples were stained with Alizarin Red S for calcite identification and non-calcareous samples were stained for feldspar identification. Each thin section was also injected with blue epoxy to help identify porosity.

Thin section analysis was completed under plane-polarized and cross-polarized light on a Leica Motic BA300Pol. Photomicrographs were obtained with a linked Leica DMC5400 camera. Thin sections were analyzed to provide additional insight into the processes affecting the samples during time of deposition. Petrographic analysis included a visual assessment of Wentworth grain size classes, roundness, sorting, porosity, depositional features, and mineralogy. Descriptions from outcrop and thin section are reported in Tables 2 and 3. Additional data from hXRF and grain morphological analysis help to support the generalized petrographic classification.

3.3 hXRF Analysis

X-ray fluorescence (XRF) spectroscopy is a widely used and a well-established non-destructive method for estimating bulk geochemistry of major elements (Mg, Al, Si, P, K, Ca, Ti, Mn, Fe) and minor elements of the sample (Fisher et al., 2014; Lemiere, 2018; Oyedotun, 2018). XRF is a low cost and rapid physical technique, which analyzes major and trace elemental abundance regardless of chemical bonds (Lemiere, 2018). XRF measurements can be influenced by analyzing weathered versus nonweathered faces, uneven or highly fractured surfaces, porosity, moisture, diagenetic minerals, and grain size variability (Fisher et al., 2014; Oyedotun, 2018). These limitations may be mitigated by conducting repeated shot intervals on a clean rock face or when the samples are naturally fine grained and homogenous (Fisher et al., 2014; Lemiere, 2018). Measurement accuracy can be improved throughout data collection by calibrating to a known standard (Lemiere, 2018).

Raw samples were initially analyzed for major and trace elements using the Olympus Vanta handheld X-ray fluorescence (hXRF) instrument prior to processing. Samples were washed then thoroughly air-dried to obtain a clean surface for a detailed geochemical analysis via the “point-and-shoot” technique discussed by Lemiere (2018). All hXRF data was collected using the same beam parameters, with beam one firing for 30 seconds and beam two firing for 60 seconds. Approximately ten hXRF analyses were taken from various locations on each sample, to obtain an accurate representation of the bulk geochemistry. hXRF data and associated measurement uncertainties are reported in parts-per-million (ppm) for 34 elements. Samples with increased Zr (ppm) were selected for U-Pb geochronology to optimize chances for zircon recovery. Abundances of light elements measured for each sample are strongly influenced by porosity and are removed from the total elemental abundance calculations.

3.4 Mineral Separation

Detrital zircon samples were processed using a new method for mineral separation designed specifically for silt-sized material with carbonate cement and increased pyrite content (modified from Dickinson and Gehrels, 2008; Simpson et al., 2012; Gehrels and Pecha, 2014; Thomas et al., 2014; Andò, 2020). First, the samples were coarsely disaggregated by crushing via a jaw crusher. Crushed samples with a high carbonate content were then washed in a 3 mol hydrochloric (HCl) acid bath to remove carbonate cement, optimizing the chances for successful disaggregation and zircon recovery.

All samples were disaggregated into silt-sized sediment via a wet mortar and pestle hand crushing technique (Andò, 2020). This approach involved gently pulverizing small amounts of crushed sample at a time, using an up and down motion with the sample submerged in a thin layer of deionized water. After approximately 15-20 repetitions of pulverizing, the silt was decanted through a sieve cloth to prevent the disaggregated grains from being destroyed by continuous crushing. Wet sieving of all disaggregated material was completed using 15 μm sieve cloth for fine silt and clay removal, following Andò (2020). After sieving, samples were separated via heavy liquid density separation using sodium polytungstate (SPT) at a density of 2.90 g/cm^3 . Using liquid nitrogen, the dense fraction was partially frozen to be recovered separately from the low-density fraction. Approximately 10% of the dense fraction was saved for heavy mineral analysis, if desired in future studies, while the remaining 90% continued to magnetic separation.

Initial removal of magnetic minerals was achieved using a neodymium hand magnet, followed by the final separation utilizing the Frantz magnetic separator set at 0.5A, 1.0A, and 1.5A, respectively. The remaining non-magnetic residuals were run through a final round of

heavy liquid density separation using methylene iodide (MEI) at a density of 3.32 g/cm³. Several pyrite-rich samples underwent a nitric acid (HNO₃) wash to remove pyrite from the zircon separate. The nitric acid wash followed the procedure outlined in the mineral separation instruction manual prepared by Simpson et al. (2012). Upon completion of mineral separation, concentrated zircon separates were mounted to 1” round pucks using double sided tape.

3.5 High Resolution Grain Imaging

Grain mounts were imaged invoking a cost-effective method of high-resolution imaging for grains in the silt-sized fraction. This method follows a simplistic approach utilizing a Leica Z16 APO macroscope outfitted with the Leica DMC 5400 linked camera, a mechanical stage, and the Leica KL 1500 LCD ring light attachment. Grain mounts were affixed to the mechanical stage using tape just covering the outer edge of the puck, allowing the mount to move with the mechanical stage and maintain precision throughout image collection. However, a simple 3D printed holder could easily be made in the future to eliminate the need for tape as a means of affixing the mount to the stage. The ring light was attached above the stage. Macroscopic images were acquired with the Leica Application Suite X (version 3.014.23224) with a magnification of 6.3x. The LASX automatic brightness adjustment was used when capturing images; therefore, variations in color were observed from image to image. Each mount was imaged using a vertical snake-like pattern moving up-down and right to left, ensuring enough overlap to be effectively stitched together. Sample images were stitched together within Adobe Photoshop 2020. For this study, high resolution images were used to map the grain mounts for U-Pb analysis and to evaluate grain morphology.

3.6 Detrital Zircon U-Pb Geochronology

Zircon (ZrSiO_4) has proven to be a highly useful geochronometer as a result of its durability and aptness for radiometric dating (Košler and Sylvester, 2003). Uranium (U) can replace Zr within zircon's crystal lattice. Radioactive decay of ^{238}U to ^{206}Pb and ^{235}U to ^{207}Pb provide the basis for measuring the timing of zircon crystallization (Gehrels et al., 2006, 2008; Gehrels and Pecha, 2014). Several key isotope ratios, $^{206}\text{Pb}/^{238}\text{U}$, $^{207}\text{Pb}/^{235}\text{U}$, and $^{207}\text{Pb}/^{206}\text{Pb}$, are routinely measured in detrital zircon geochronology, typically via laser ablation mass spectrometry (Gehrels et al., 2006, 2008; Gehrels and Pecha, 2014). Age precision varies depending upon which ratio is used. The $^{206}\text{Pb}/^{238}\text{U}$ age typically has higher precision for younger (<1.2 Ga) analyses, while the $^{207}\text{Pb}/^{206}\text{Pb}$ age is typically more precise for older (>1.2 Ga) analyses (Gehrels, 2014). Secondary zircon standards are measured throughout data collection to provide an estimate of the accuracy of isotopic readings.

Uranium-lead (U-Pb) geochronology of individual zircon grains was conducted using an iCAP quadrupole inductively-coupled plasma mass spectrometer (Q-ICP-MS) via laser ablation at the University of Arkansas Trace Element and Radiogenic Isotope Laboratory (TRAIL) facilities. Zircon grains were selected at random for analysis, using either a 30- μm -, 25- μm -, or 15- μm -diameter spot size depending upon grain size. Analyses were conducted with one U-Th-Pb measurement per grain. The zircon standard 91500 (1065 Ma; Wiedenbeck et al., 2004) was used as a primary standard. Two secondary zircon standards, R33 (419 Ma; Black et al., 2004) and Plešovice (337 Ma; Sláma et al., 2008), were used to measure the accuracy of isotopic readings.

Data reduction was accomplished using Igor Pro—Iolite V3.1 (Paton et al., 2011; Fisher et al., 2017). Rim and core analyses were identified within Iolite and are reported accordingly.

Isotopic ratios were plotted on a concordia plot to assess the degree of concordance for each analysis. Data are filtered for discordance using the following guidelines as a cut-off: >15% for $^{206}\text{Pb}/^{238}\text{U}$ ages and >30% or <15% for $^{207}\text{Pb}/^{206}\text{Pb}$ ages. Discordant analyses were removed prior to plotting. Discordant analyses are often attributed to the mobilization of Pb after the crystallization of the zircon, the mixing of separate age domains within the same analysis, or some combination of the two (Gehrels et al., 2006; Gehrels et al., 2008; Gehrels and Pecha, 2014).

Detrital zircon U-Pb age data were plotted within detritalPy (v1.3), a Python-based toolset for visualizing and analyzing detrital geo-thermochronologic data (Sharman et al., 2018). Detrital age distributions are plotted as cumulative distribution functions (CDFs), probability density plots (PDPs), kernel density estimations (KDEs), histograms, and pie diagrams. Relative age distribution plots were created by plotting KDEs using a bandwidth of 10 Myr. Multi-dimensional scaling (MDS) plots for individual samples or groups of samples demonstrate the level of similarity between each sample in the dataset (Vermeesch, 2013; Sharman et al., 2018).

3.7 Detrital Zircon Morphology

Analysis of zircon morphology is a useful quantitative tool that can further refine provenance interpretations and improve understanding of processes influencing the grains from source to sink (Gärtner et al., 2013; Makuluni et al., 2019; Yue, 2019). Makuluni et al. (2019) inferred the two major controls of zircon grain shape to be the original melt environment from which the zircon crystallized and the sedimentary transport system that modified the zircon crystal. Markwitz and Kirkland (2018) substantiated the claim that a strong quantitative relationship between zircon grain shape and age exists and is directly tied to the source, regardless of hydrologic sorting initiated by sediment transport.

Images of zircons can be quantified through a variety of grain measurements, including dimensions of the major axis and the minor axis (Markwitz and Kirkland, 2018; Makuluni et al., 2019). Further statistical quantification can be completed using the fore-mentioned measurements, including aspect ratio $\left[\frac{\text{major axis}}{\text{minor axis}}\right]$ and axial ratio $\left[\frac{\text{minor axis}}{\text{major axis}}\right]$ (Markwitz and Kirkland, 2018; Makuluni et al., 2019). The minor axes of zircon crystals have been shown by Markwitz and Kirkland (2018) to experience less alteration caused by sedimentary transportation compared to the major axes, thus the minor axes should more strongly reflect the character of the magmatic source from which the grain crystallized. Elongated and angular morphologies may be indicative of non-recycled zircons from an igneous source (Gärtner et al., 2013). Higher rates of physical abrasion via recycling and long-distance transport causes increasing roundness in older and farther traveled zircon grains (Gärtner et al., 2013).

Zircon grain morphologies were quantified using the high-resolution grain images of the mounted zircon separates. Grains which were analyzed for U-Pb geochronology from all 19 detrital zircon samples were assessed for the major axis (long), minor axis (short), sphericity, roundness, and euhedrism. To measure the grain axes, two separate lines were drawn on each individual grain. The major (long) axis of each grain was measured initially, while the minor (short) axis was measured perpendicular to and intersecting the major axis. Sphericity and roundness were visually assessed utilizing visual classification charts for particle shape (from Krumbein and Sloss, 1963; Powers, 1953). Euhedrism was assessed visually using the diagram for euhedral, subhedral, and anhedral grains from Nesse (2011). Grain color assessment was not possible for this study due to color variation within a given sample caused by the LASX automatic brightness adjustment. It is possible for color to be assessed in future studies if the user sets the brightness for the entirety of image collection for each sample, respectively.

Chapter 4: Results

4.1 Petrographic Analysis

Detailed petrographic assessments were conducted for all nineteen samples. General sample descriptions were completed prior to sample processing (Table 2). Detailed microscopic analysis of thin sections enhanced the general field description for each sample (Table 3). Thorough descriptions of lithologic facies are reported for both the Dewey County and Canadian County cores in greater detail by Gates (2020).

Variations in lithology were identified among samples, including samples derived from the same vertical core. Samples range from very fine-lower silt to medium-lower sand with an average grain size of very fine silt. All samples were enriched in monocrystalline quartz, with variable bioclastic, carbonate, and clay content. Mud-rich samples (e.g., Dewey-1 and Canadian-1) typically displayed thin laminations, little-to-no bioturbation, and little-to-no skeletal fragments. Samples composed largely of a carbonate-rich matrix (e.g., Dewey-4 and Canadian-3) displayed a higher degree of variation in depositional features and skeletal fragment content. Typical depositional features included thinly laminated bedding, graded bedding, planar and inclined laminations, and varying degrees of bioturbation. Samples can be further divided into groups according to clay content and sedimentary structures, listed as follows in order of decreasing clay content.

MRFD-01 is a black, calcareous, argillaceous, and fissile shale. Dewey-1, Canadian-1, MRFD-02, and MRFD-03 are dark gray-brown, calcareous, argillaceous siltstones with thin planar laminations. Dewey-1 and Canadian-2 are dark gray-brown, calcareous, argillaceous siltstones with thin planar and inclined laminations.

PQ-04 and PQ-01 are both light gray, calcareous and thinly laminated siltstones. PQ-01 is also slightly bioclastic. Canadian-5 is a dark gray-black, poorly laminated, slightly bioclastic, argillaceous, and calcareous siltstone.

Dewey-5, Canadian-4, and Dewey-3 are bioturbated, slightly argillaceous and calcareous siltstones. Dewey-4 and Dewey-2 are both stylolitic calcareous siltstones; however, Dewey-4 contains bioclasts that form planar laminations and Dewey-2 is heavily bioturbated.

ES-1, S-15, and Canadian-3 are light gray, calcareous siltstones. ES-1 and S-15 display thin planar laminations, whereas Canadian-3 is relatively homogeneous.

CNY-1 and BTVL-01 are brown-yellow, quartz-rich sandstones. CNY-1 has planar laminations and is finer-grained than BTVL-01, which is cross-bedded and coarser-grained.

4.2 hXRF Analysis

Each of the 19 samples were assessed in detail (approximately ten measurements per sample) for elemental composition using hXRF. All hXRF data are reported in the Supplementary Data File (Tables S1 and S2). The average elemental concentration of each sample was calculated and used for interpretation of whole rock geochemistry. Geochemical variations correspond to lithologic variations. Quartz-rich samples display a high proportion of Si, clay-rich samples commonly display a higher proportion of Al, and carbonate-rich samples commonly display a higher proportion of Ca (Fig. 5).

hXRF data indicate that the average concentration of light elements (LE) is roughly 60%, with a range from 54% to 66%. LE abundances, which are influenced by porosity, were excluded from the total element concentration; data reported below are renormalized following exclusion of LE. Significant element concentrations (>5%) measured in each sample include Si, Ca, and Al

(together accounting for ~93% of the total) (Fig. 5). Minor proportions (>2% and <5%) of Fe, K, S, Ti, and P are also noted (together accounting for ~6% of the total) (Fig. 5).

When hXRF elemental concentrations are plotted on an MDS plot, subtle variations in each sample can be identified (Fig. 5). Variations in geochemistry between samples are predominantly related to variations in Si, Ca, and Al concentrations, which likely relate to variability in proportions of quartz, carbonate, and clay content. Three clusters can be identified on the MDS plot (Fig. 5). The first group (MRFD-01, -02, -03; PQ-01, -04; Canadian-3; and Dewey-4) is made up of calcareous, quartz-rich siltstones and shale that are enriched in Ca (48% on average) and Si (41% on average) with lower proportions of Al (5% on average) (Fig. 5). The second group (Dewey-1,-2,-3,-5; Canadian-1,-2,-4,-5; ES-1; and S-15) are moderately calcareous, quartz-rich siltstones that have a lower Ca content (20% on average) and a higher Si (64% on average) and Al (8% on average) content relative to the first group (Fig. 5). Group three (BTVL-01 and CNY-1) are mostly composed of Si (90% on average) with nominal Al (6% on average). Both of those samples are quartz-rich sandstones of Chesterian age (Fig. 5).

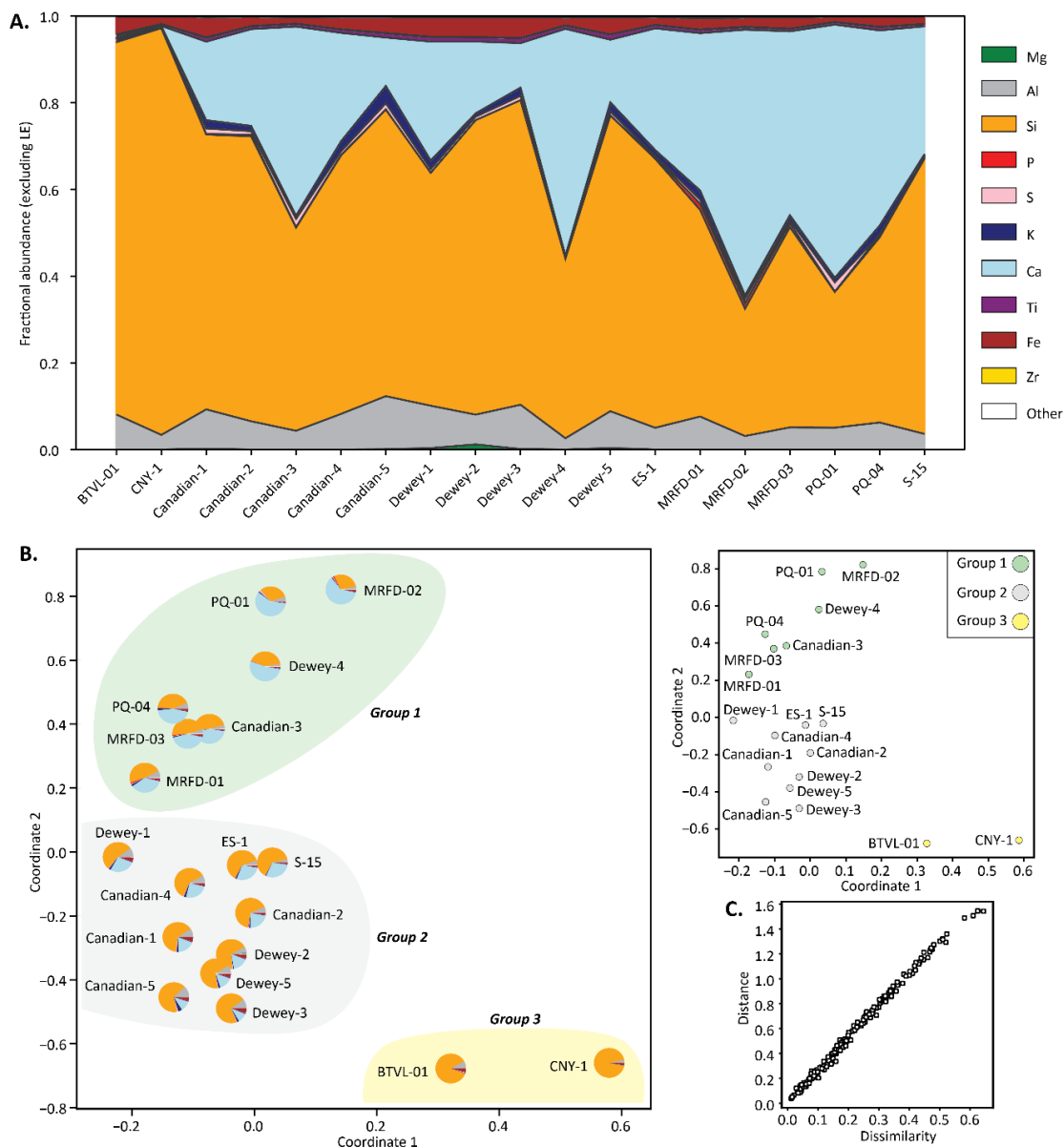


Figure 5. (A) Stacked plot of hXRF fractional abundances for each sample. Samples contain high proportions of Si, Ca, and Al. “Other” elements include V, Cr, Mn, Co, Ni, Cu, Zn, As, Se, Rb, Sr, Y, Nb, Mo, Ag, Cd, Sn, Sb, W, Hg, Pb, Bi, and Th. (B) MDS plots (left and upper right) display relative similarities and differences in geochemistry for each sample. The MDS plot (left) displays the geochemical abundances for each sample shown as pie diagrams, using the same color scheme as above (A). Samples were divided into 3 groups based on lithologic distinctions. Group 1 samples (green) are quartz- and carbonate-rich siltstones and shale with high concentrations of Si and Ca. Group 2 samples (gray) are less calcareous than Group 1 samples and are more argillaceous siltstones, which contain higher concentrations of Al. Group 3 samples (yellow) are quartz-rich sandstones with high concentrations of Si. (C) Shepard plot shows a good correlation between sample dissimilarity and distance on the MDS plot.

4.3 Detrital Zircon U-Pb Geochronology

Nineteen detrital zircon samples yielded 2478 concordant U-Pb age analyses and all data are reported in the Supplementary Data File (Fig. 6 and Table S3). Analyses were filtered to be within the acceptable limits of concordance using the criteria described in the methods section 3.6. Rim and core data were reported as separate analyses when applicable (Fig. 7 and Table S3).

Major age fractions were interpreted from known geologic provinces and prominent age peaks in the dataset (Fig. 4; Xie et al., 2018; Lawton et al., 2021; Thomas et al., 2021): Appalachian (240-500 Ma); peri-Gondwanan terranes (500-900 Ma); Grenville (900-1350 Ma); Granite-Rhyolite province (1350-1600 Ma); undivided provinces from 1600-2500 Ma, including the Yavapai-Mazatzal province (1600-1800 Ma), Trans-Hudson/Penokean orogens (1800-1900 Ma), and Trans-Amazonian Eburnean craton (1900-2250 Ma); and Superior craton (2500-3200 Ma).

All 19 Upper Mississippian samples are, on average, largely composed of both Grenville grains (c.a. 900-1350 Ma; average of 32%) and Appalachian grains (c.a. 240-500 Ma; average of 21%) (Fig. 6). Along with these Laurentian sources, a significant proportion of peri-Gondwanan grains (c.a. 500-900 Ma; average of 17%) are also present in these Upper Mississippian samples (Fig. 6). Pre-Grenville age categories account for the remaining zircon, including contributions from undivided provinces (c.a. 1600-2500 Ma; average of 13%), the Granite-Rhyolite province (c.a. 1350-1600 Ma; average of 12%), and the Superior craton (c.a. 2500-3200 Ma; average of 4%) (Fig. 6).

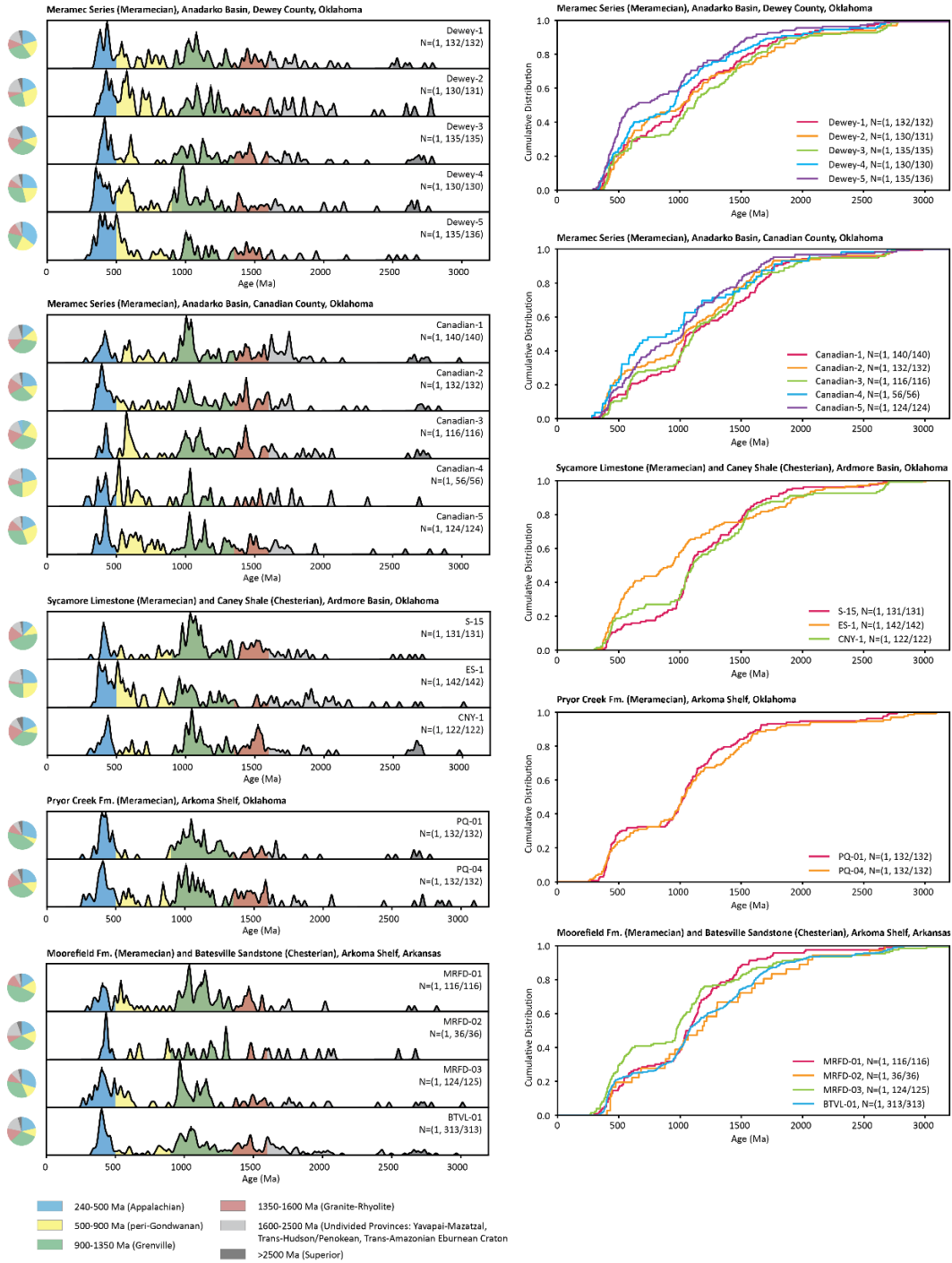


Figure 6. Detrital zircon relative age distribution plots (left) and cumulative age distribution plots (right) of study samples. Relative age distribution plot types are kernel density estimation (KDE) plots constructed using a bandwidth of 10 Myr. X/Y notation indicates the number of analyses plotted (X) versus the total number of analyses in the sample (Y). Meramecian samples contain significant proportions of Grenville (900-1350 Ma), Appalachian (240-500 Ma), and peri-Gondwanan (500-900 Ma).

Prominent peri-Gondwanan age peaks are observed in Dewey-1 (836 Ma), Dewey-2 (552 and 576 Ma), Dewey-3 (605 Ma), Dewey-5 (501 and 558 Ma), Canadian-3 (574 Ma), Canadian-4 (520 Ma), Canadian-5 (540 Ma), ES-1 (508 Ma), and MRFD-01 (540 Ma). Samples Canadian-4, Dewey-2, and ES-1 have the largest fraction of peri-Gondwanan grains (c.a. 500-900 Ma), making up 29%, 27%, and 25% of each sample, respectively.

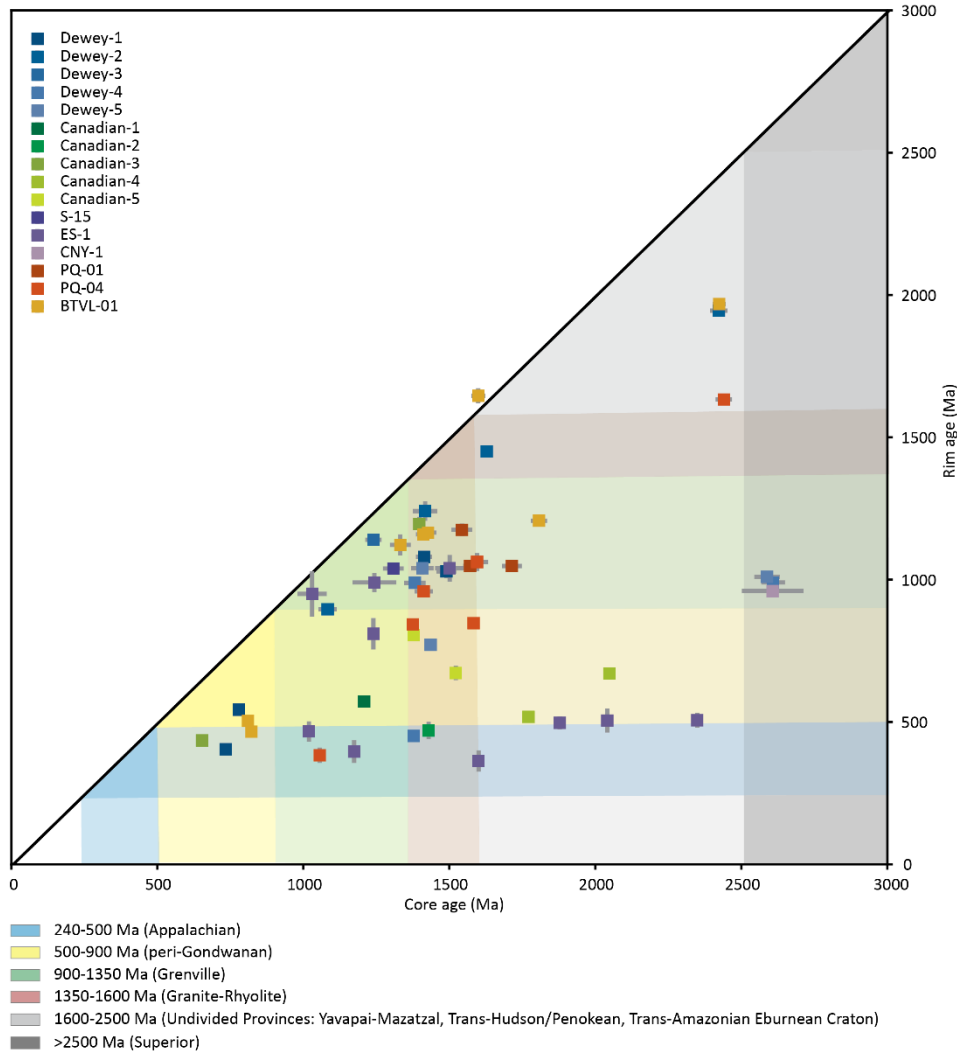


Figure 7. Detrital zircon rim and core data of study samples, with highlighted geologic provinces used for provenance interpretation.

A total of 62 grains have discernable rim and core relationships (Fig. 7 and Table S3). Zircons with peri-Gondwanan (c.a. 240-500 Ma) cores have rims that are peri-Gondwanan and Appalachian (c.a. 240-500 Ma) (Fig. 7). Zircons with peri-Gondwanan rims span a broad range

of core ages (500-2500 Ma) (Fig. 7). Grenville rims make up the largest fraction of reported rim and core data and are common on 900-1350 Ma and 1350-1600 Ma cores (Fig. 7).

4.3.1 Anadarko Basin (Canadian and Dewey Counties)

The Dewey County core samples (Dewey-1, -2, -3, -4, -5), representative of the thinner, shallow-water deposits of the Meramec Series, are comprised of Grenville grains (c.a. 900-1350 Ma; average of 27%), Appalachian grains (c.a. 240-500 Ma; average of 24%) and peri-Gondwanan grains (c.a. 500-900 Ma; average of 20%) (Fig. 6). Dewey-1 has increased proportions of Grenville (30%), Appalachian (20%), and peri-Gondwanan (20%) grains, with conspicuous age peaks at 433, 539, 733, 836, 1024, 1078, 1447, and 1613 Ma. Smaller (maximum of 3 analyses per peak) peri-Gondwanan age peaks also include 507, 509, 572, 652, and 786 Ma. Peri-Gondwanan grains are most abundant in Dewey-2, comprising 27% of the total sample, as well as Grenville (22%) and Appalachian (19%) grains. Notable age peaks for Dewey-2 include 463, 552, 576, 1012, 1083, 1184, and 1237 Ma. Additionally, several smaller (maximum of 4 analyses per peak) peri-Gondwanan peaks are also identified at 552, 576, 616, 690, 736, and 840 Ma. Dewey-3 has a lower proportion of peri-Gondwanan (12%) grains and higher proportions of Grenville (30%) and Appalachian (21%) grains, with significant age peaks at 416, 605, 973, 1038, 1126, 1393, 1465, and 1718 Ma. Dewey-4 has a substantial fraction of Grenville (30%), Appalachian (25%), and peri-Gondwanan (22%) grains. Dewey-4 has conspicuous age peaks at 353, 503, 522, 582, 919, 982, 1123, 1383, and 1650 Ma, along with two smaller peri-Gondwanan age peaks (maximum of 3 analyses per peak) at 618 and 752 Ma. Dewey-5 has a greater proportion of Appalachian (35%) grains versus Grenville (21%) and peri-Gondwanan (21%) grains, with prominent age peaks present at 383, 417, 501, 558, 1005, 1036, 1088, 1355, and 1441 Ma.

The Canadian County core samples (Canadian-1, -2, -3, -4, -5), derived from the thicker, deep-water deposits of the Meramec Series, produced significant proportions of Grenville (c.a. 900-1350 Ma; average of 30%), peri-Gondwanan (c.a. 500-900 Ma; average of 21%), Appalachian (c.a. 240-500 Ma; average of 17%), undivided provinces (c.a. 1600-2500 Ma; average of 15%), and Granite-Rhyolite (c.a. 1350-1600 Ma; average of 14%) zircon (Fig. 6). Grenville grains make up the most significant proportion of the Canadian County samples, apart from Canadian-4 which is enriched in peri-Gondwanan grains (29%). Canadian-1 yields notable proportions of Grenville (34%), undivided provinces (c.a. 1600-2500 Ma; 21%), Appalachian (14%), and peri-Gondwanan (14%) grains, with prominent age peaks of 963, 1007, 1041, 1434, 1455, 1622, and 1750 Ma (Fig. 6). Three smaller peri-Gondwanan age peaks (maximum of 4 analyses per peak) include 561, 594, and 731 Ma (Fig. 6). Canadian-2 displays an age signature similar to Canadian-1 consisting of Grenville (30%), Appalachian (23%), and peri-Gondwanan (14%) grains. Conspicuous age peaks include 395, 950, 1031, 1139, 1393, 1439, 1596, and 1755 Ma; in addition, a smaller (maximum of 3 analyses per peak) peri-Gondwanan age peak is present at 502 Ma (Fig. 6). Canadian-3 and Canadian-5 display similar age fraction abundances and age peaks. Canadian-3 is comprised of Grenville (34%), peri-Gondwanan (20%), and Appalachian (10%) grains, with age peaks of 426, 574, 1002, 1025, 1106, 1435, 1574, and 1623 Ma (Fig. 6). Canadian-5 is similarly composed of Grenville (31%), peri-Gondwanan (26%), and Appalachian (19%) grains, with age peaks of 423, 540, 1030, 1139, 1314, 1510, and 1651 Ma; in addition, five smaller peri-Gondwanan age peaks (maximum of 4 analyses per peak) are present at 603, 640, 676, 758, and 799 Ma (Fig. 6). Canadian-4 is enriched in peri-Gondwanan grains which comprise 29% of the total sample, in addition to Grenville (21%), and Appalachian (21%)

grains. Conspicuous age peaks for Canadian-4 include 520 and 1034 Ma, with several smaller (maximum of 3 analyses per peak) peri-Gondwanan peaks at 584 and 647 Ma (Fig. 6).

4.3.2 Ardmore Basin (Sycamore and Caney)

Samples from the Ardmore Basin (S-15, ES-1, CNY-1) contain a large proportion of Grenville grains (c.a. 900-1350 Ma; average of 36%), although ES-1 contains an equal abundance of peri-Gondwanan grains (c.a. 500-900 Ma; average of 25%) (Fig. 6). S-15 and CNY-1 have similar age fraction proportions, including Grenville (S-15, 45%; CNY-1, 37%), Appalachian (S-15, 12%; CNY-1, 19%), and peri-Gondwanan (S-15, 11%; CNY-1, 8%) grains (Fig. 6). S-15 has distinguishable peak ages of 406, 1034, 1069, 1512, and 1531 Ma; additionally, two smaller peri-Gondwanan peaks (maximum of 4 analyses per peak) include 532 and 804 Ma (Fig. 6). CNY-1 conversely has fewer age peaks including 438, 1004, 1044, 1106, and 1523 Ma, along with two smaller peri-Gondwanan peaks (maximum of 3 analyses per peak) are present at 611 and 716 Ma (Fig. 6). ES-1 has a more evenly distributed grain age distribution that includes Grenville (25%), peri-Gondwanan (25%), and Appalachian (24%) grains, with age peaks of 373, 508, 830, 953, 993, 1040, and 1870 Ma (Fig. 6). ES-1 also contains several smaller peri-Gondwanan age peaks (maximum of 5 analyses per peak) including 544, 580, 621, 691, and 703 Ma (Fig. 6).

4.3.3 Arkoma Shelf (Pryor Creek)

Samples from the northern fringe of the Arkoma Basin in Oklahoma contain a high proportion of Grenville (PQ-01, 44%; PQ-04, 33%) and Appalachian (PQ-01, 29%; PQ-04, 23%) grains (Fig. 6). PQ-04 contains significant proportions of Granite-Rhyolite 1350-1600 Ma (17%) and peri-Gondwanan (13%) grains, while PQ-01 has a more muted peri-Gondwanan signature (6%). PQ-01 has age peaks at 400, 427, 988, 1017, 1046, 1098, 1471, and 1555 Ma (Fig. 6). PQ-

04 displays age peaks at 406, 842, 954, 1008, 1055, 1450, and 1584 Ma, along with 4 smaller peri-Gondwanan peaks (maximum of 3 analyses per peak) at 555, 592, 622, and 733 Ma (Fig. 6).

4.3.4 Arkoma Shelf (Moorefield and Batesville)

Meramecian samples from the northern fringe of the Arkoma Basin in eastern Arkansas (MRFD-01, -02, -03) are comprised of Grenville (average of 38%), Appalachian (average of 22%), and peri-Gondwanan (average of 14%) zircons (Fig. 6). MRFD-01 and MRFD-02 have similar abundances of Grenville (MRFD-01, 47%; MRFD-02, 33%), Appalachian (MRFD-01, 16%; MRFD-02, 19%), and peri-Gondwanan (MRFD-01, 16%; MRFD-04, 14%) grains. MRFD-03 contains high proportions of Grenville (34%) and Appalachian (30%) zircons, with a significant proportion of peri-Gondwanan (14%) grains. Prominent age peaks from MRFD-01 include 407, 540, 961, 1035, 1119, 1150, and 1467 Ma, as well as a smaller peri-Gondwanan peak (maximum of 3 analyses per peak) present at 580 Ma (Fig. 6). MRFD-02 has only yielded 36 concordant grain analyses, resulting in a less well-constrained definition of age peaks, which occur at 433, 672, 879, 1191, 1301, and 1481 Ma (Fig. 6). MRFD-03 has age peaks of 353, 402, 494, 968, 1092, 1157, and 1495 Ma, with the addition of 2 smaller peri-Gondwanan peaks (maximum of 3 analyses per peak) present at 539 and 594 Ma (Fig. 6). BTVL-01 is the Chesterian Batesville sandstone from the same locality as the Moorefield samples. However, sample BTVL-01 displays a lower proportion of peri-Gondwanan grains (10%) and increased concentrations of Grenville (32%), Appalachian (21%), undivided provinces 1600-2500 Ma (17%), and Granite-Rhyolite (15%) grains relative to the Moorefield samples. Prominent age peaks within BTVL-01 include 401, 460, 972, 1048, 1161, 1390, 1477, and 1602 Ma (Fig. 6).

4.4 Zircon Morphological Analysis

A total of 2429 zircon grains were assessed for morphologic characteristics, including the major grain axis length, minor grain axis length, sphericity, roundness, and euhedrism.

Morphological data are reported in the Supplementary Data File (Table S4). Qualitative grain morphology analyses (i.e., sphericity, roundness and euhedrism) vary systematically with respect to grain age (Fig. 8). Generally, older zircon grains have higher sphericity and roundness, which is expected for older grains that have been continually recycled and degraded over time (Fig. 8). Euhedrism also follows a similar trend, as younger age fractions contain increased proportions of euhedral zircon grains compared to the large proportion of anhedral grains within the older age fractions (Fig. 8). Of the 2429 zircon grains recovered, anhedral are most abundant (50%),

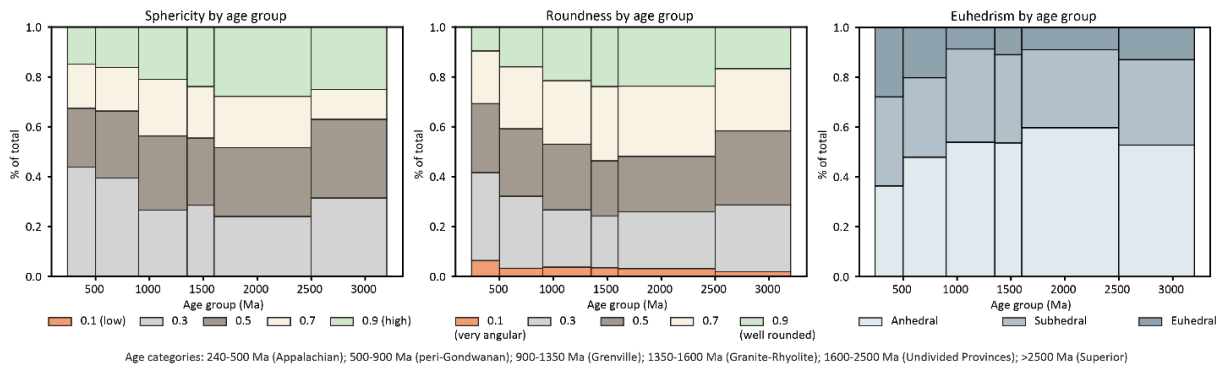


Figure 8. Zircon sphericity (left), roundness (middle), and euhedrism (right) displayed as fractional abundance within six zircon age categories. Both grain sphericity and grain roundness increase with increasing age. Older grains also tend to be more anhedral than younger grains.

followed by subhedral (35%), and euhedral (15%).

Quantitative morphological characteristics (i.e., major axis, minor axis, aspect ratio, and axial ratio) were compared against the age of the zircons (Table S4; Fig. 9). Grains that are 500-900 Ma (peri-Gondwanan) display a modest difference in major and minor axis dimensions than the younger (Appalachian, 240-500 Ma) and older (>900 Ma) grains. Grains in the peri-Gondwanan fraction have a median major axis length of 57 μm , while younger and older grains

have median values from 61-65 μm (Fig. 9). Despite being less pronounced, the minor axis length shows the same relationship as the major grain axis. Peri-Gondwanan grains have a median minor axis of 37 μm , while grains of the other geologic fractions range from 40-44 μm (Fig. 9). The overall aspect ratio generally decreases with increasing age, while the axial ratio is simply the inverse relationship and increases with increasing age (Fig. 9).

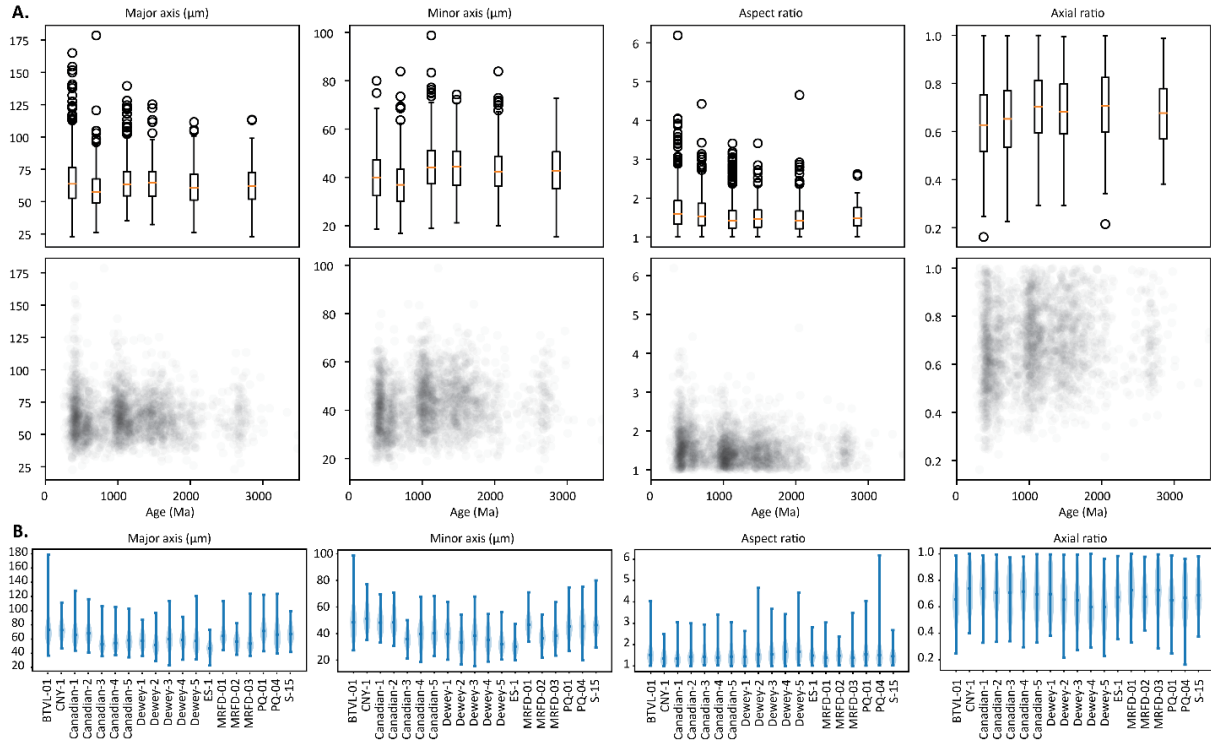


Figure 9. Comparison of grain dimensions versus age: major axis (left), minor axis (left-middle), aspect ratio (right-middle), and axial ratio (right). **(A)** Morphological characteristics versus grain age, shown with box and whisker plots (upper) and point plots (lower). **(B)** Violin plots showing morphological characteristics for each sample. Grains of peri-Gondwanan age (500-900 Ma) display smaller major and minor grain axes.

Chapter 5: Discussion

5.1 Provenance of Meramecian Silt

Variation in provenance is evident with respect to time and space through Late Mississippian and into Early Pennsylvanian time. Comparison of new zircon age data to previously published samples of Chesterian and Early Pennsylvanian age from the craton of

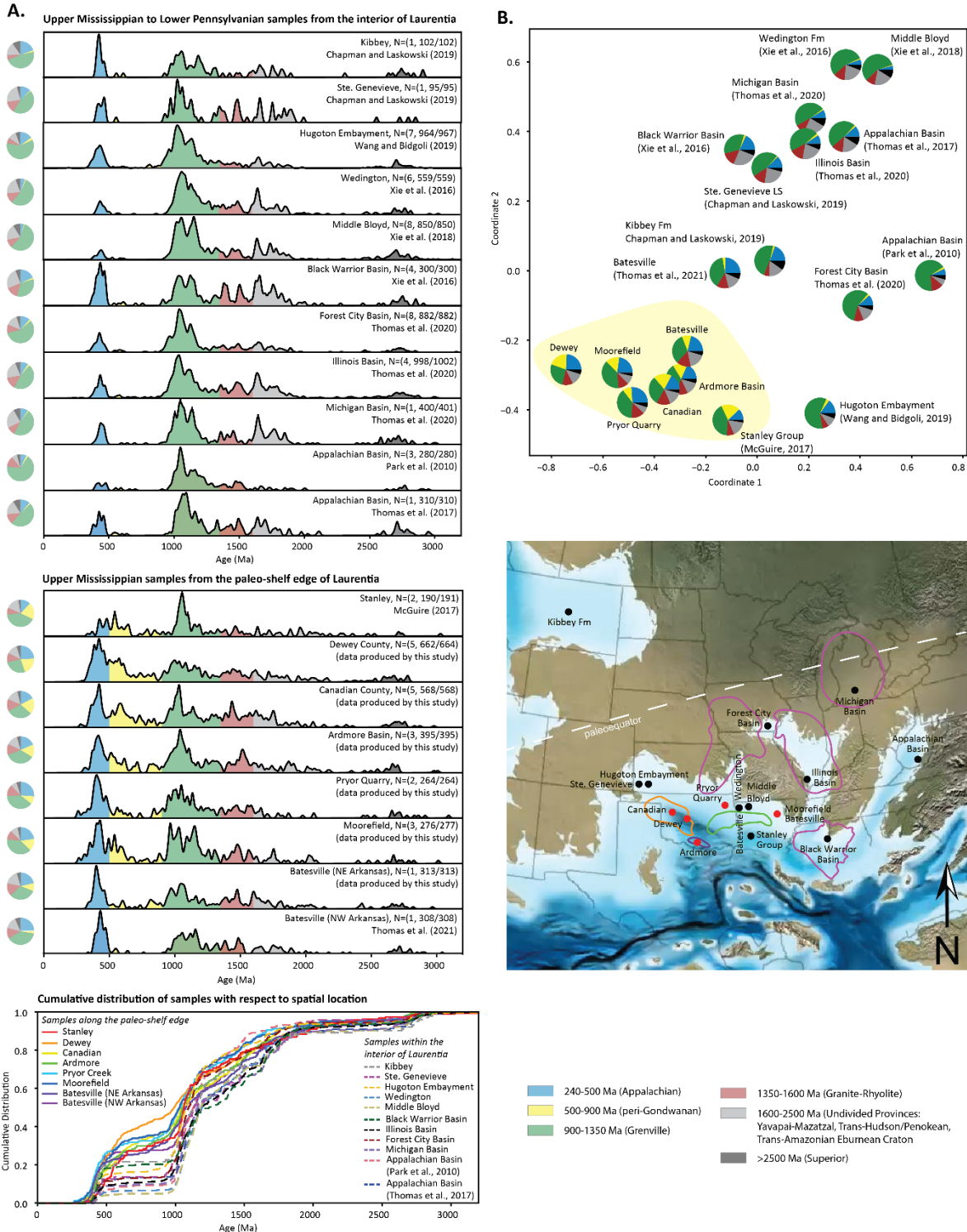


Figure 10. (A) Relative and cumulative age distribution plots of published and study zircon data. Samples are separated by spatial location with respect to the paleo-shelf edge of Laurentia. **(B)** Age data plotted on an MDS plot (right) shows the spatial control on the presence of peri-Gondwanan grains. Samples located along the paleo-shelf edge are clustered together (highlighted yellow) and display significant peri-Gondwanan grain proportions.

Laurentia shows contrasting detrital zircon U-Pb ages, particularly with respect to grains interpreted to have been derived from peri-Gondwanan terranes (500-900 Ma) (Park et al, 2010; Xie et al., 2016a; Xie et al., 2016b; McGuire, 2017; Thomas et al., 2017; Xie et al., 2018; Chapman and Laskowski, 2019; Wang and Bidgoli, 2019; Thomas et al., 2020; Thomas et al., 2021) (Figs. 10 and 11). Published sample data are reported in the Supplementary Data File (Table S5).

Silt-sized peri-Gondwanan zircon grains are prominently found in marine sediments deposited along the southern paleo-shelf edge of Laurentia (Fig. 11). Age-equivalent and near age-equivalent (Chesterian to Lower Pennsylvanian) samples located on the craton of Laurentia do not possess a significant proportion of 500-900 Ma grains (3% on average) (Fig. 11). For example, fluvial-deltaic deposits coming from the craton of Laurentia, including the Wedington Sandstone (Xie et al., 2016a) and the Middle Bloyd Sandstone (Xie et al., 2018), do not contain abundant 500-900 Ma grains. Of the 48 previously published detrital zircon samples compiled in this study, only sample ST-26, a light gray, fine to medium grained, quartz-rich sandstone from the Meramecian to Chesterian Stanley Group contains a significant proportion (39%) of 500-900 Ma (peri-Gondwanan) grains (McGuire, 2017). The Stanley Group, which is comprised of mainly turbidite sandstones and shales interbedded with volcanoclastics, was deposited from east-to-west in deep-water south of the paleo-shelf edge (Suneson, 2012; McGuire, 2017).

The notable lack of peri-Gondwanan grains from Upper Mississippian to Lower Pennsylvanian units on the Laurentian craton can be observed on a MDS plot, as samples from the continental interior and paleo-shelf edge plot in different regions (Fig. 10). Samples located along the paleo-shelf edge of Laurentia are clustered in the lower left-hand portion of the MDS plot and are highlighted in yellow (Fig. 10). Chesterian samples on the craton of Laurentia do not

possess the fraction of peri-Gondwanan grains that the Meramecian and finer-grained Chesterian samples on the paleo-shelf edge possess.

Detrital zircon U-Pb data supports the hypothesis that Upper Mississippian silt originated from both Laurentian and peri-Gondwanan sources (Fig. 6). The Meramecian silts deposited along the paleo-shelf edge are prominently sourced from the Grenville (32%), Appalachian (21%), and peri-Gondwanan (16%) geologic provinces, suggesting that sediment was sourced from both the Appalachian Orogen and peri-Gondwanan terranes to the south and/or east (Figs. 10 and 11). Increasing contributions of peri-Gondwanan grains occurs further south along the paleo-shelf edge, with decreasing proportions in samples towards the craton (Figs. 10 and 11).

5.2 Sedimentary Transport Pathways

Laurentian sourced grains were likely eroded via fluvial processes from the Appalachian highlands and transported from east to west across Laurentia (Fig. 11; Chapman and Laskowski, 2019; Thomas et al., 2020; Lawton et al., 2021; Thomas et al., 2021). However, fluvial transport of Appalachian and Grenville detritus across the craton to the Arkoma, Ardmore, and Anadarko basins was unlikely, due to the vast epicontinental sea that covered parts of Laurentia and would have created a barrier for rivers (Chapman and Laskowski, 2019). Furthermore, models of exclusively fluvial transport for Upper Mississippian silt do not account for the presence of grains sourced from the southerly and/or easterly peri-Gondwanan terranes (Price et al., 2020; Thomas et al., 2020; Lawton et al., 2021).

Sediment production from peri-Gondwanan terranes escalated during the early stages of collision between Gondwana with the southeastern edge of Laurentia (Lawton et al., 2021;

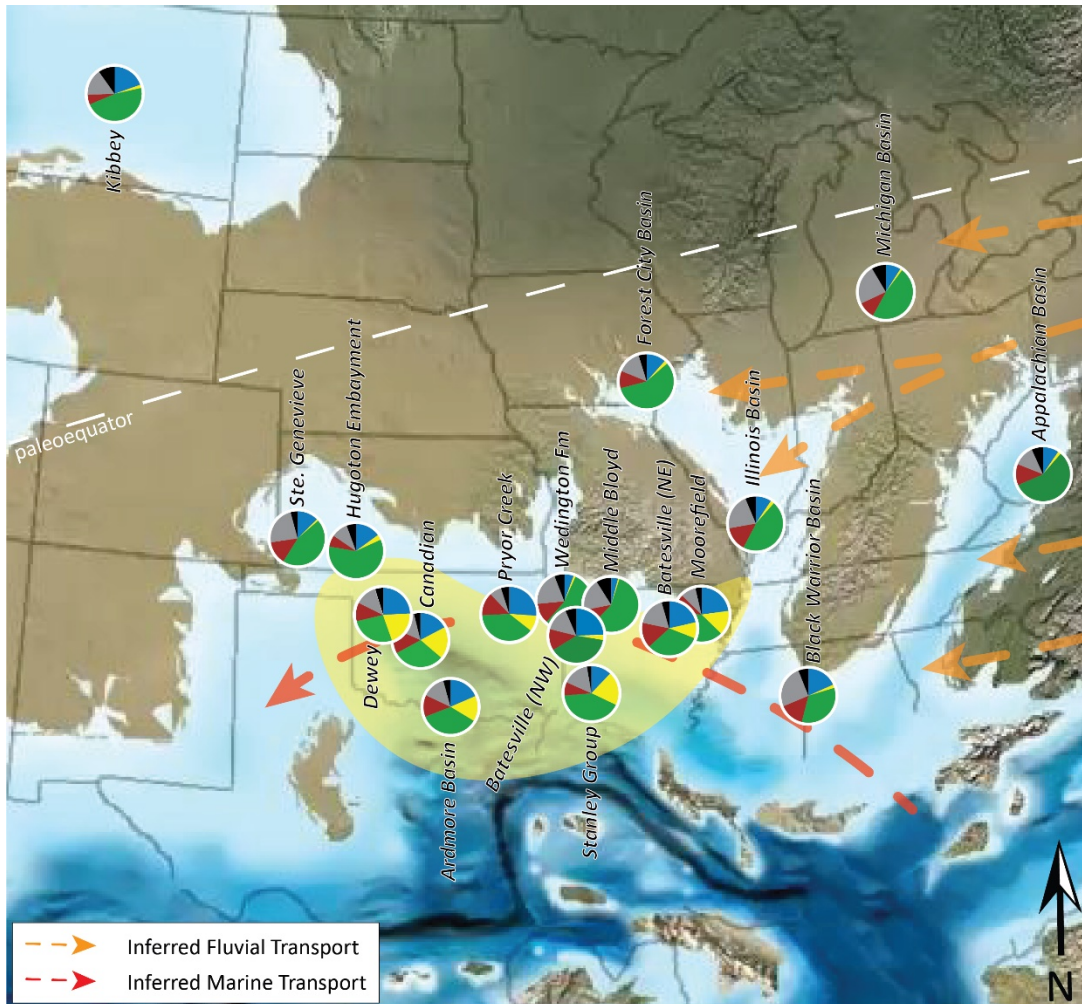


Figure 11. Grouped study and published zircon data (pies), plotted spatially on a paleogeographic reconstruction of Laurentia during Late Mississippian time. Samples with a pronounced peri-Gondwanan affinity are highlighted by yellow shading. Meramecian samples along the paleoshelf of Laurentia display significant proportions of peri-Gondwanan grains while still containing a substantial proportion of Grenville and Appalachian grains, implying a mixed provenance. Therefore, sediment transport pathways are inferred to include both Laurentian sources (Appalachian Orogen) and terranes to the south and/or east (peri-Gondwanan). Sediment from peri-Gondwanan terranes was transported from east to west along the southern paleoshelf edge via marine currents. Sediment from the Appalachian highlands was transported by rivers from the east-northeast, with finer-grained sediments potentially being carried further west by contour-parallel marine currents.

Thomas et al., 2021). Increased sediment production, spurred by tectonic convergence, would have produced great quantities of silt and sand during Upper Mississippian time (Lawton et al., 2021; Thomas et al., 2021). Silt produced from peri-Gondwanan terranes had potential to

transport via aeolian processes, driven by the paleo-tradewinds from the southeast (Lawton et al., 2021; Thomas et al., 2021). Gregorich et al. (2018) previously proposed that silt comprising the Borden siltstone may have been carried by winds during dust storms and monsoon events. McGlannan et al. (2019) also proposed that silt comprising the Woodford Shale, Sycamore Formation, and the lower Caney Shale was carried across the Laurentian craton by winds.

Aeolian transport would facilitate widespread distribution of fine-grained silts across Laurentia. However, the silt-sized peri-Gondwanan zircons are limited to the paleo-shelf edge (Fig. 11). If aeolian processes were responsible for the transport of silts onto the Laurentian craton, then silt-sized peri-Gondwanan zircons should be distributed widely within basins of southern Laurentia. Thus, the lack of peri-Gondwanan zircon grains in samples located inland of the Laurentian paleo-shelf edge suggests these 500-900 Ma grains were not delivered by aeolian processes.

Peri-Gondwanan zircons are distinctively smaller than grains sourced from Laurentian provinces, likely reflecting a different transport pathway for detritus that was sourced farther away from the depositional setting (Figs. 8 and 9; Lawton et al., 2021). Grains between the ages of 500-900 Ma (peri-Gondwanan) generally have smaller major and minor grain axes with increased sphericity, implying the detritus was transported a greater distance, thus supporting a long-distance transport model in line with marine transport (Figs. 8 and 9). Silt can be carried a longer distance via marine currents compared to coarser sand that tends to be deposited closer to its source.

Marine currents would have enabled grains in the silt-size fraction to be transported over a greater distance following the paleo-shelf edge of Laurentia prior to settling out of suspension (Chapman and Laskowski, 2019; Lawton et al., 2021). Appalachian silts may have been

transported by fluvial processes closer in proximity to the source and transported along the paleo-shelf margin via marine currents (Chapman and Laskowski, 2019; Lawton et al., 2021; Thomas et al., 2021). Fluvial models showing a north to south transport pathway (e.g., Price et al., 2020) lack an explanation for the significant proportions of peri-Gondwanan grains that are present along the paleo-shelf given the lack of these grains on the craton (Fig. 1). Chapman and Laskowski (2019) proposed a marine transport model, inferring that Appalachian-derived sediments traveled via marine currents from east to west along the paleo-shelf edge of Laurentia (Fig. 1). However, this interpretation does not address the presence of peri-Gondwanan grains along the Laurentian paleo-shelf edge. In this study, peri-Gondwanan grains are proposed to have traveled via contour-parallel currents from east to west along the paleoshelf edge of Laurentia and mixed with fluvial input from the Appalachian Orogen to the north and northeast (Fig. 11).

The low-angle, stacked, prograding clinoform structures that form the Oklahoma STACK play have been inferred to be fluvial in origin forming via a subaqueous delta (Price et al., 2020). However, the abundance of peri-Gondwanan grains in the STACK play siltstones suggests that these deposits were not exclusively sourced from rivers that emanated from North America (Figs. 1 and 11). Instead, the results from this study suggest that the low-angle clinoforms of the STACK play may have been influenced by contour-parallel marine currents, similar to those that produce contourite deposits (Rebesco et al., 2014; Shelley, 2016; Hardwick, 2018; Miller, 2018; Gates, 2020; Price et al., 2020). Contourites form along the continental slope, with contour currents transporting and depositing sediments along the slope edge (Rebesco et al., 2014). The stratal geometries created by some contour currents are perhaps not inconsistent with the stacked, low-angle, southeastward prograding clinoforms observed by past workers in the STACK play

(Price et al., 2017; Hardwick, 2018; Miller, 2018; and Price et al., 2020). A better understanding of how these clinoforms formed would provide insight into what processes drove sediment transport along the Upper Mississippian paleo-shelf edge of Laurentia.

Chapter 6: Conclusions

6.1 Conclusions

This study utilized a multi-proxy approach to provenance analysis including hXRF, petrography, detrital zircon U-Pb geochronology and grain morphology of Upper Mississippian siltstones, including samples from the Meramecian-aged STACK play of the Anadarko Basin and its regional equivalents in eastern Oklahoma and Arkansas. Quantitative and qualitative assessments of detrital zircon grains including 2478 U-Pb age analyses from nineteen samples provide several insights into provenance and sediment transport pathways of the Meramecian silts. The principal findings of the study are:

1. The origin of silt-sized detritus during the Meramecian was not limited to purely Laurentian sources. The Meramec silts of the STACK play and age-equivalent strata along the paleo-shelf edge contain detritus sourced from both the easterly Appalachian highlands of Laurentia and the southerly peri-Gondwanan terranes, which is indicative of source mixing. Contributions from peri-Gondwanan sources account for approximately 17% of the zircons in siltstone deposited along the paleo-shelf edge of Laurentia.
2. Silt produced from peri-Gondwanan terranes was likely transported from the east to the west along the Laurentian paleo-shelf edge via contour parallel marine currents. Detritus sourced from the Appalachian Orogeny was transported via rivers, delivered into the shallow epicontinental sea via river deltas, and partially transported along the Laurentian paleo-shelf

edge via contour parallel currents. Overall, a shorter transport distance of Appalachian detritus is suggested by larger zircon grain sizes relative to those of peri-Gondwanan origin.

References

- Alemán-Gallardo, E. A., Ramírez-Fernández, J. A., Rodríguez-Díaz, A. A., Velasco-Tapia, F., Jenchen, U., Cruz-Gámaz, E. M., De León-Barragán, L., Navarro-De León, I., 2019, Evidence for an Ordovician continental arc in the pre-Mesozoic basement of the Huizachal–Peregrina Anticlinorium, Sierra Madre Oriental, Mexico: *Peregrina Tonalite. Mineralogy and Petrology*. 113, 505–525.
- Andò, S., 2020, Gravimetric Separation of Heavy Minerals in Sediments and Rocks. *Minerals*, 10(3), 273, <https://doi.org/10.3390/MIN10030273>.
- Becker, T. P., Thomas, W. A., Samson, S. D., and Gehrels, G. E., 2005, Detrital zircon evidence of Laurentian crustal dominance in the lower Pennsylvanian deposits of the Alleghanian clastic wedge in eastern North America. *Sediment. Geol.* 182, 59–86.
- Becker, T. P., Thomas, W. A., and Gehrels, G. E., 2006, Linking late Paleozoic sedimentary provenance in the Appalachian basin to history of Alleghanian deformation. *Am. J. Sci.* 306, 777–798.
- Black, L. P., Kamo, S. L., Allen, C. M., Davis, D. W., Aleinikoff, J. N., Valley, J. W., Mundil, R., Campbell, I. H., Koehn, R. J., Williams, I. S., Foudoulis, C., 2004, Improved ²⁰⁶Pb/²³⁸U microprobe geochronology by the monitoring of a trace-element-related matrix effect; SHRIMP, ID-TIMS, ELA-ICP-MS and oxygen isotope documentation for a series of zircon standards. *Chem. Geol.* 205, 115–140. <https://doi.org/10.1016/j.chemgeo.2004.01.003>.
- Blakey, R., 2020, Paleogeography and Geologic Evolution of North America, NAU Geology. DeepTimeMaps™, from <https://deeptimemaps.com/>.
- Chapman, A. D., and Laskowski, A. K., 2019, Detrital zircon U-Pb data reveal a Mississippian sediment dispersal network originating in the Appalachian orogen, traversing North America along its southern shelf, and reaching as far as the southwest United States. *Lithosphere* ; 11 (4): 581–587, <https://doi.org/10.1130/L1068.1>.
- Cullen, A., 2017, Devonian-Mississippian Petroleum Systems of Southern Laurasia: What Makes the STACK-MERGE-SCOOP in Oklahoma so Special? *AAPG Playmaker Forum* Oklahoma City, OK.
- Cullen, A., 2019, My favorite....thin section: The Caney sandstone from Philip's Creek— one of Rick Andrews' favorite outcrops: *Shale Shaker*, v. 70, no. 4, p. 168-180.
- Dickinson, W. R., and Gehrels, G. E., 2003, U-Pb Ages of detrital zircons from Permian and Jurassic eolian sandstones of the Colorado Plateau, USA: Paleogeographic implications. *Sediment. Geol.* 163, 29–66.

- Dickinson, W. R., and Gehrels, G. E., 2008, U-Pb Ages of Detrital Zircons in Relation to Paleogeography: Triassic Paleodrainage Networks and Sediment Dispersal Across Southwest Laurentia. *Journal of Sedimentary Research*, 78(12), 745-764.
- Dickinson, W. R., and Lawton, T. F., 2001, Carboniferous to Cretaceous assembly and fragmentation of Mexico. *Geol. Soc. Am. Bull.* 113, 1142–1160.
- Evans, J. E., Soreghan, M., 2015, Long-distance sediment transport and episodic resedimentation of Pennsylvanian dust (eolian silt) in cave passages of the Mississippian Leadville Limestone, southwestern Colorado, USA. In: Feinberg, J., Gao, Y., Alexander Jr., E.C. (Eds.), *Caves and Karst Across Time*. Geological Society of America Special Paper 516, Boulder, Colorado, pp. 263-283.
- Fisher, C. M., Paton, C., Pearson, D. G., Sarkar, C., Luo, Y., Tersmette, D. B., and Chacko, T., 2017, Data reduction of laser ablation split-stream (LASS)analyses using newly developed features within iolite: With applications to Lu-Hf 1 U-Pb in detrital zircon and Sm-Nd 1U-Pb in igneous monazite. *Geochemistry, Geophysics, Geosystems*,18, 4604–4622, <https://doi.org/10.1002/2017GC007187>.
- Fisher, L., Gazley, M., Baensch, A., Barnes, S., Cleverley, J., and Duclaux, G., 2014, Resolution of geochemical and lithostratigraphic complexity: A workflow for application of portable X-ray fluorescence to mineral exploration. *Geochemistry: Exploration, Environment, Analysis*. 14, <https://doi.org/10.1144/geochem2012-158>.
- Frazier, W.J., and Schwimmer, D.R., 1987, Regional Stratigraphy of North America. 719 pp. *Plenum Press*, New York, <https://doi.org/10.1007/978-1-4613-1795-1>.
- Fritz, R. D., and Mitchell, J. R., 2021, The Anadarko “Super” Basin: 10 key characteristics to understand its productivity. *AAPG Bulletin*, 105(6), 1199–1231, <https://doi.org/10.1306/03242120082>.
- Gärtner, A., Linnemann, U., Sagawe, A., Hofmann, M., Ullrich, B., and Kleber, A., 2013, Morphology of zircon crystal grains in sediments—characteristics, classifications, definitions. *Geol. Saxonica*, 59, 65–73.
- Gates, D., 2020, Integrated Hyperspectral and Geochemical Analysis of the Upper Mississippian Meramec STACK Play and Outcrop Equivalents, Anadarko Basin and Ozark Uplift, Oklahoma. *M.S. thesis*, University of Arkansas, Fayetteville, Arkansas.
- Gehrels, G., 2014, Detrital Zircon U-Pb Geochronology Applied to Tectonics. *Annual Review of Earth and Planetary Sciences*, 42(6), 479-482.
- Gehrels, G.E., Blakey, R., Karlstrom, K.E., Timmons, J.M., Dickinson, B., and Pecha, M., 2011, Detrital zircon U-Pb geochronology of Paleozoic strata in the Grand Canyon, Arizona: *Lithosphere*, v. 3, p. 183–200, <https://doi.org/10.1130/L121.1>.

- Gehrels, G., and Pecha, M., 2014, Detrital zircon U-Pb geochronology and Hf isotope geochemistry of Paleozoic and Triassic passive margin strata of western North America. *Geosphere*, 10(1), 49-65, <https://doi.org/10.1130/GES00889.1>.
- Gehrels, G., Valencia, V., and Pullen, A., 2006, Detrital Zircon Geochronology by Laser-Ablation Multicollector ICPMS at the Arizona LaserChron Center. *The Paleontological Society Papers*, 12, 67-76, <https://doi.org/10.1017/S1089332600001352>.
- Gehrels, G. E., Valencia, V. A., and Ruiz, J., 2008, Enhanced precision, accuracy, efficiency, and spatial resolution of U-Pb ages by laser ablation–multicollector–inductively coupled plasma–mass spectrometry, *Geochem. Geophys. Geosyst.*, 9, Q03017, <https://doi.org/10.1029/2007GC001805>.
- Godwin, C., 2010, Review of the Upper Mississippian Mayes Group (Meramecian and Chesterian) of northeastern Oklahoma, *GSA Abstracts with Programs*, v. 42, no. 2, p. 41.
- Godwin, C.J., 2017, Lithostratigraphy and Conodont Biostratigraphy of the Upper Boone group and Mayes Group in the Southwestern Ozarks of Oklahoma, Missouri, Kansas, and Arkansas.
- Gregorich, H., McLaughlin, P. I., Malone, D., and Craddock, J., 2018, Evidence for long distance eolian transport of 1460 Ma zircons in the Borden siltstone, Illinois Basin, USA. An abstract presented at the *GSA annual meeting*, Indianapolis, IN.
- Gutschick, R. C., and Sandberg, C. A., 1983, Mississippian Continental Margins of the Conterminous United States, in Stanley, D. J., and Moore, G. T. (eds.), *The Shelfbreak: Critical Interface on Continental Margins. Society of Economic Paleontologists and Mineralogists*, Special Publication 33, p. 79-86.
- Hardwick, J., 2018, Reservoir Quality Evaluation of the Meramec and Upper Osage Units in the Anadarko Basin. doi:10.1093/imamci/dnt037.
- Hatcher Jr., R. D., Thomas, W. A., Geiser, P. A., Snoke, A. W., Mosher, S., Wiltschko, D. V., 1989, Alleghanian orogen. In: Hatcher Jr., R. D., Thomas, W. A., Viele, G. W. (Eds.), *The Geology of North America*, Volume F-2. The Appalachian–Ouachita Orogen in the United States. Geological Society of America, Boulder, Colorado, pp. 233–318.
- Hickman, G., 2018, Parasequence-Scale Stratigraphic Variability of Lithology and Porosity of Mississippian Meramec Reservoirs and the Relationships to Production Characteristics, STACK Trend, Oklahoma.
- Higley, D., 2013, 4D Petroleum System Model of the Mississippian System in the Anadarko Basin Province. *Mountain Geologist*. 50. 81-98.

- Johnson, K. S., and Cardott, B. J., 1992, Geologic framework and hydrocarbon source rocks of Oklahoma, in K.S. Johnson and B.J. Cardott, eds., Source rocks in the southern Midcontinent, 1990 symposium: *OGS Circular* 93, p. 21-37.
- Keppie, J. D., Dostal, J., Murphy, J. B., and Nance, R. D., 1996, Terrane transfer between eastern Laurentia and western Gondwana in the early Paleozoic: Constraints on global reconstructions. In: Nance, R.D., Thompson, M.D. (Eds.), Avalonian and Related Peri-Gondwanan Terranes of the Circum-North Atlantic. *Geological Society of America Special Paper* 304, Boulder, Colorado, pp. 369–380.
- Košler, J., Sylvester, P. J., 2003, Present Trends and the Future of Zircon in Geochronology: Laser Ablation ICPMS. *Reviews in Mineralogy and Geochemistry*; 53 (1): 243–275, <https://doi.org/10.2113/0530243>.
- Krumbein, W. C., and Sloss, L. L., 1963, Stratigraphy and sedimentation (2nd. Edition): San Francisco, W. H. Freeman and Co.
- Lawlor, P. J., Ortega-Gutiérrez, F., Cameron, K. L., Ochoa-Camarillo, H., Lopez, R., and Sampson, D. E., 1999, U–Pb geochronology, geochemistry, and provenance of the Grenvillian Huiznopala Gneiss of eastern Mexico. *Precambrian Res.* 94, 73–99.
- Lawton, T. F., Blakey, R. C., Stockli, D. F., & Liu, L. (2021). Late Paleozoic (Late Mississippian–Middle Permian) sediment provenance and dispersal in western equatorial Pangea. *Palaeogeography, Palaeoclimatology, Palaeoecology*, 572, 110386. <https://doi.org/10.1016/j.palaeo.2021.110386>
- Leary, R. J., Umhoefer, P., Smith, M. E., T. M., Saylor, J. E., Riggs, N., Burr, G., Lodes, E., Foley, D., Licht, A., Mueller, M. A., and Baird, C., 2020, Provenance of Pennsylvanian–Permian sedimentary rocks associated with the Ancestral Rocky Mountains orogeny in southwestern Laurentia: Implications for continental-scale Laurentian sediment transport systems. *Lithosphere* 2020; 12 (1): 88–121. doi: <https://doi.org/10.1130/L1115.1>
- Lemiere, B., 2018, A Review of hXRF (Field Portable X-ray Fluorescence) Applications for Applied Geochemistry. *Journal of Geochemical Exploration, Elsevier*, [ff10.1016/j.gexplo.2018.02.006](https://doi.org/10.1016/j.gexplo.2018.02.006). [ffhal-01740950f](https://doi.org/10.1016/j.gexplo.2018.02.006).
- Lopez, R., Cameron, K. L., Jones, N. W., 2001, Evidence for Paleoproterozoic, Grenvillian, and Pan-African age Gondwanan crust beneath northeastern Mexico. *Precambrian Res.* 107, 195–214.
- Makuluni, P., Kirkland, C. L., and Barham, M., 2019, Zircon grain shape holds provenance information: A case study from southwestern Australia. *Geological Journal* 54, 1279–93.
- Manger, W. L., 2014, An introduction to the Lower Mississippian (Kinderhookian-Osagean) geology of the southern Ozarks, Guidebook. Fayetteville, AR: University of Arkansas.

- Markwitz, V., and Kirkland, C. L., 2018, Source to sink zircon grain shape: Constraints on selective preservation and significance for Western Australian Proterozoic basin provenance. *Geoscience Frontiers* 9, 415–30.
- McFarland, J. D., and Bush, W. V., 2004, Stratigraphic summary of Arkansas: Little Rock, AR, *Arkansas Geological Commission*.
- McGlannan, A. J., Bonar, A. L., Pfeifer, L. S., Adams, S. M., Duarte, D. E., Totten, C. J., Cullen, A., and Soreghan, G. S., 2019, A Model for the Origin of Devonian-Mississippian Mudrocks in Greater Midcontinent North America. An abstract presented at the *GSA annual meeting*, Phoenix, AZ.
- McGuire, P.R., 2017, U-Pb Detrital Zircon Signature of the Ouachita Orogenic Belt, *M.S. thesis*: Fort Worth, Texas, Texas Christian University, 78 p.
- McKee, J. W., Jones, N. W., and Anderson, T. H., 1999, The late Paleozoic and early Mesozoic history of the Las Delicias terrane, Coahuila, Mexico. In: Bartolini, C., Wilson, J. L., Lawton, T. F. (Eds.), *Mesozoic Sedimentary and Tectonic History of North Central Mexico. Geological Society of America Special Paper* 340, Boulder, Colorado, pp. 161–189.
- Miller, J., and Cullen, A., 2018, My favorite outcrop: Sycamore formation I-35 south, arbutle mountains, OK. *Shale Shak*. 69 (No 2), 87-99.
- Miller, J. C., Pranter, M. J., and Cullen, A. B., 2018, Regional Stratigraphy and Organic Richness of the Mississippian Meramec and Associated Strata, Anadarko Basin, Central Oklahoma, 70(2), 50–79.
- Nance, D. A., 2018, Structural Cross Sections and Subsurface Maps of the Atoka Formation in the Northern Arkoma Basin, Western and Northwestern Arkansas.
- Nesse, W., 2011, Introduction to Mineralogy, Oxford: *Oxford University Press*.
- Northcutt, R. A., and Campbell, J. A., 1995, Geologic Provinces of Oklahoma Map. *Oklahoma Geological Survey*. http://www.ogs.ou.edu/geolmapping/Geologic_Provinces_OF5-95.pdf.
- Ortega-Gutiérrez, F., Ruiz, J., and Centeno-García, E., 1995, Oaxaquia, a Proterozoic microcontinent accreted to North America during the late Paleozoic. *Geology* 23, 1127–1130.
- Oyedotun, T. D. T., 2018, X-ray fluorescence (XRF) in the investigation of the composition of earth materials: a review and an overview, *Geology, Ecology, and Landscapes*, 2:2, 148-154, <https://doi.org/10.1080/24749508.2018.1452459>.

- Park, H., Barbeau Jr., D., Rickenbaker, A., Bachmann-Krug, D., and Gehrels, G., 2010, Application of Foreland Basin Detrital-Zircon Geochronology to the Reconstruction of the Southern and Central Appalachian Orogen. *The Journal of Geology*, 118(1), 23-44, <https://doi.org/10.1086/648400>.
- Paton, C., Hellstrom, J., Paul, B., Woodhead, J., and Hergt, J. 2011, Iolite: Freeware for the Visualisation and Processing of Mass Spectrometric Data. *J. Anal. At. Spectrom.* VL - IS -. online. 10.1039/C1JA10172B.
- Patruno, S., and Helland-Hansen, W., 2018, Clinoforms and clinoform systems: Review and dynamic classification scheme for shorelines, subaqueous deltas, shelf edges and continental margins. *Earth-Science Reviews*; 185: 202-233, <https://doi.org/10.1016/j.ea3irev.2018.05.016>.
- Pindell, J. L., and Kennan, L., 2009, Tectonic evolution of the Gulf of Mexico, Caribbean and northern South America in the mantle reference frame: an update. In: James, K.H., Lorente, M.A., Pindell, J.L. (Eds.), *The Origin and Evolution of the Caribbean Plate. Geological Society, London, Special Publication 328*, pp. 1–55.
- Poole, F. G., Perry Jr., W. J., Madrid, R. J., Amaya-Martínez, R., 2005, Tectonic synthesis of the Ouachita-Marathon-Sonora orogenic margin of southern Laurentia: Stratigraphic and structural implications for timing of deformational events and plate-tectonic model. In: Anderson, T. H., Nourse, J. A., McKee, J. W., Steiner, M. B. (Eds.), *The Mojave-Sonora Megashear Hypothesis: Development, Assessment, and Alternatives. Geological Society of America Special Paper 393*, Boulder, Colorado, pp. 543–596.
- Powers, M. C., 1953, A new roundness scale for sedimentary particles. *Journal of Sedimentary Research*; 23 (2): 117–119, <https://doi.org/10.1306/D4269567-2B26-11D7-8648000102C1865D>.
- Price, B., Haustveit, K., Lamb, A., 2017, Influence of Stratigraphy on Barriers to Fracture Growth and Completion Optimization in the Meramec Stack Play, Anadarko Basin, Oklahoma. *Proc. 5th Unconv. Resour. Technol. Conf.* 1–8, <https://doi.org/10.15530/urtec2017-2697585>.
- Price, B. J., Pollack, A. C., Lamb, A. P., Peryam, T. C., and Anderson, J. R., 2020, Depositional interpretation and sequence stratigraphic control on reservoir quality and distribution in the Meramecian Sooner trend Anadarko Basin, Canadian, and Kingfisher Counties (STACK) play, Anadarko Basin, Oklahoma, United States. *AAPG Bulletin*; 104 (2): 357–386, <https://doi.org/10.1306/04301917411>.
- Raith, M., Raase, P., and Reinhardt, J., 2011, *Guide to Thin Section Microscopy. University of Bonn.*

- Rebesco, M., Hernández-Molina, F. J., Van Rooij, D., and Wåhlin, A., 2014, Contourites and associated sediments controlled by deep-water circulation processes: State-of-the-art and future considerations. *Marine Geology*, 352, 111-154.
- Sharman, G. R., Sharman, J. P., and Sylvester, Z., 2018, detritalPy: A Python-based toolset for visualizing and analysing detrital geo-thermochronologic data. *The Depositional Record*, v. 4, p. 202–215, <https://doi.org/10.1002/dep2.45>.
- Shelley, S. A., 2016, Outcrop-Based Sequence Stratigraphy and Reservoir Characterization of an Upper Mississippian Mixed Carbonate- Siliciclastic Ramp, Mayes County, Oklahoma. *M.S. thesis*, Oklahoma State University, Stillwater, Oklahoma, 75 p.
- Simpson, G., Pecha, M., and Gehrels, G., 2012, Mineral Separation Instruction Manual. Tucson; *Arizona LaserChron Center*. p. 15-16, retrieved from <https://drive.google.com/file/d/0B9ezu34P5h8eYzRmZGYwMGItMGI1MC00MGQ3LWE4YzEtNWZiZmFiNDQ5OGRh/view?resourcekey=0-5BMGpY7CQ1UwgnbRSYFa9A>.
- Sláma, J., Košler, J., Condon, D. J., Crowley, J. L., Gerdes, A., Hanchar, J. M., Horstwood, M. S. A., Morris, G. A., Nasdala, L., Norberg, N., Schaltegger, U., Schoene, B., Tubrett, M. N., Whitehouse, M. J., 2008, Plešovice zircon—a new natural reference material for U-Pb and Hf isotopic microanalysis. *Chem Geol.* 249:1-35. <https://doi.org/10.1016/j.chemgeo.2007.11.005>.
- Snedden, J. W., and Galloway, W. E., 2019, The Gulf of Mexico Sedimentary Basin. *Cambridge University Press*, Cambridge, 326 pp.
- Suneson, N. H., 2012, Arkoma Basin Petroleum - Past, Present, and Future. *Shale Shaker*, 63(1), 38–70.
- Thomas, W. A., 2011, Detrital-zircon geochronology and sedimentary provenance. *Lithosphere*, 3(4), 304–308. <https://doi.org/10.1130/RF.L001.1>.
- Thomas, W. A., and Astini, R. A., 1996, The Argentine Precordillera: A traveler from the Ouachita embayment of North American Laurentia. *Science* 273, 752–757.
- Thomas, W. A., Gehrels, G. E., Greb, S. F., Nadon, G. C., Satkoski, A. M., and Romero, M. C., 2017, Detrital zircons and sediment dispersal in the Appalachian foreland. *Geosphere*, v. 13, no. 6, p. 2206–2230, <https://doi.org/10.1130/GES01525.1>.
- Thomas, W. A., Gehrels, G. E., Sundell, K. E., Greb, S. F., Finzel, E. S., Clark, R. J., Malone, D. H., Hampton, B. A., and Romero, M. C., 2020, Detrital zircons and sediment dispersal in the eastern Midcontinent of North America. *Geosphere*, v. 16, no. 3, p. 817– 843, <https://doi.org/10.1130/GES02152.1>.

- Thomas, W. A., Gehrels, G. E., Sundell, K.E., and Romero, M.C., 2021, Detrital-zircon analyses, provenance, and late Paleozoic sediment dispersal in the context of tectonic evolution of the Ouachita orogen. *Geosphere*, v. 17, no. X, p. 1–34, <https://doi.org/10.1130/GES02288.1>.
- Vermeesch, P., 2013, Multi-sample comparison of detrital age distributions. *Chemical Geology*, 341(341), 140–146. <https://doi.org/10.1016/j.chemgeo.2013.01.010>.
- Yue, W., Yue, X., Zhang, L., Liu, X., and Song, J., 2019, Morphology of Detrital Zircon as a Fingerprint to Trace Sediment Provenance: Case Study of the Yangtze Delta. *Minerals*, 9(7), 438, <https://doi.org/10.3390/min9070438>.
- Wang, W., and Bidgoli, T. S., 2019, Detrital zircon geochronologic constraints on patterns and drivers of continental-scale sediment dispersal in the Late Mississippian. *Geochemistry, Geophysics, Geosystems*, 20, 5522– 5543, <https://doi.org/10.1029/2019GC008469>.
- Warner, G., 2019, Stratigraphy and Depositional Characterization of the Moorefield Shale (Middle-Late Mississippian) in its Type Area, Northeastern Arkansas (Eastern Arkoma Basin). *Theses and Dissertations*, retrieved from <https://scholarworks.uark.edu/etd/3305>.
- Wiedenbeck, M., Hanchar, J. M., Peck, W. H., Sylvester, P., Valley, J., Whitehouse, M., Kronz, A., Morishita, Y., Nasdala, L., Fiebig, J., Franchi, I., Girard, J.-P., Greenwood, R., Hinton, R., Kita, N., Mason, P., Norman, M., Ogasawara, M., Piccoli, P., Rhede, D., Satoh, H., Schulz-Dobrick, B., Skår, O., Spicuzza, M., Terada, K., Tindle, A., Togashi, S., Vennemann, T., Xie, Q., and Zheng, Y.-F., 2004, Further Characterisation of the 91500 Zircon Crystal. *Geostandards and Geoanalytical Research*, 28: 9-39. <https://doi.org/10.1111/j.1751-908X.2004.tb01041.x>.
- Wittman, B., 2013, Subsurface Stratigraphy and Characterization of Mississippian (Osagean to Meramecian) Carbonate Reservoirs of the Northern Anadarko Shelf, North-Central Oklahoma. *Unpublished Master of Science thesis*, University of Arkansas, 80p.
- Wortman, G. L., Samson, S. D., and Hibbard, J. P., 2000, Precise U-Pb zircon constraints on the earliest magmatic history of the Carolina terrane. *J. Geol.* 108, 321–338.
- Xie, X., Cains, W., and Manger, W. L., 2016a, U–Pb detrital zircon evidence of transcontinental sediment dispersal: provenance of Late Mississippian Wedington Sandstone member, NW Arkansas. *International Geology Review*, 58:15, 1951-1966, <https://doi.org/10.1080/00206814.2016.1193775>.
- Xie, X., O'Connor, P. M, and Alsleben, H., 2016b, Carboniferous sediment dispersal in the Appalachian–Ouachita juncture: Provenance of selected late Mississippian sandstones in the Black Warrior Basin, Mississippi, United States. *Sedimentary geology*, 342, 191-201, <https://doi.org/10.1016/j.sedgeo.2016.07.007>.

Xie, X., Buratowski, G., Manger, W.L., and Zachry, D., 2018, U-Pb detrital-zircon geochronology of the middle Bloyd sandstone (Morrowan) of northern Arkansas (U.S.A.): Implications for Early Pennsylvanian sediment dispersal in the Laurentian foreland. *Journal of Sedimentary Research*, v. 88, p. 795–810, <https://doi.org/10.2110/jsr.2018.47>.

Appendix

Table 1: Summary of Study Samples

Sample_ID	Formation	Basin	Age	Age_min (Ma)	Age_max (Ma)
Dewey-1	Meramec Series	Anadarko	Meramecian	330.9	346.7
Dewey-2	Meramec Series	Anadarko	Meramecian	330.9	346.7
Dewey-3	Meramec Series	Anadarko	Meramecian	330.9	346.7
Dewey-4	Meramec Series	Anadarko	Meramecian	330.9	346.7
Dewey-5	Meramec Series	Anadarko	Meramecian	330.9	346.7
Canadian-1	Meramec Series	Anadarko	Meramecian	330.9	346.7
Canadian-2	Meramec Series	Anadarko	Meramecian	330.9	346.7
Canadian-3	Meramec Series	Anadarko	Meramecian	330.9	346.7
Canadian-4	Meramec Series	Anadarko	Meramecian	330.9	346.7
Canadian-5	Meramec Series	Anadarko	Meramecian	330.9	346.7
S-15	Sycamore Limestone	Ardmore	Meramecian	330.9	346.7
ES-1	Sycamore Limestone	Ardmore	Meramecian	330.9	346.7
CNY-1	Caney Shale	Ardmore	Chesterian	330.9	346.7
PQ-01	Pryor Creek "Lindsey Bridge" Mbr	Arkoma Shelf	Meramecian	330.9	346.7
PQ-04	Pryor Creek "Ordinance Plant" Mbr	Arkoma Shelf	Meramecian	330.9	346.7
MRFD-01	Moorefield	Arkoma	Meramecian	330.9	346.7
MRFD-02	Moorefield	Arkoma	Meramecian	330.9	346.7
MRFD-03	Moorefield	Arkoma	Meramecian	330.9	346.7
BTVL-01	Batesville Sandstone	Arkoma	Chesterian	323.2	330.9

Sample_ID	Latitude	Longitude	Sample Type	Lithology	DZ Grains	Grains for U-Pb & Morphology	DZ Analyses
Dewey-1	36.017265	-98.924534	Core	Siltstone	150	128	132
Dewey-2	36.017265	-98.924534	Core	Siltstone	150	127	130
Dewey-3	36.017265	-98.924534	Core	Siltstone	150	134	135
Dewey-4	36.017265	-98.924534	Core	Siltstone	150	127	130
Dewey-5	36.017265	-98.924534	Core	Siltstone	151	133	135
Canadian-1	35.559378	-98.046519	Core	Siltstone	150	139	140
Canadian-2	35.559378	-98.046519	Core	Siltstone	150	131	132
Canadian-3	35.559378	-98.046519	Core	Siltstone	150	114	116
Canadian-4	35.559378	-98.046519	Core	Siltstone	84	54	56
Canadian-5	35.559378	-98.046519	Core	Siltstone	150	122	124
S-15	34.351111	-97.148648	Outcrop	Siltstone	150	130	131
ES-1	34.350282	-97.148457	Outcrop	Siltstone	150	132	142
CNY-1	34.349654	-97.149479	Outcrop	Sandstone	150	121	122
PQ-01	36.256934	-95.232744	Outcrop	Siltstone	150	129	132
PQ-04	36.256934	-95.232744	Outcrop	Siltstone	150	126	132
MRFD-01	35.764223	-91.546816	Outcrop	Shale	150	116	116
MRFD-02	35.764223	-91.546816	Outcrop	Siltstone	41	36	36
MRFD-03	35.764223	-91.546816	Outcrop	Siltstone	150	125	124
BTVL-01	35.738466	-91.622237	Outcrop	Sandstone	350	305	313

Note: Core locations are generalized to county coordinates

Table 2: Summary of Hand Sample Petrography

Sample_ID	Formation	Lithofacies	Rock Description
Dewey-1	Meramec	Calcareous Laminated Argillaceous Siltstone	black-dark brown color, thinly laminated (planar and inclined), well-sorted, calcareous (strong reaction to HCL), increased clay/mud content
Dewey-2	Meramec	Bioturbated Calcareous Siltstone	mottled light-gray color, heavily bioturbated, little to no preserved bedding features, stylolite's prominent, calcareous (strong reaction to HCL), well sorted
Dewey-3	Meramec	Laminated Bioturbated Bioclastic Calcareous Siltstone	light-dark gray color, thinly laminated (planar and inclined), partially bioturbated, calcareous (strong reaction to HCL), few shell fragments and bioclasts, well sorted
Dewey-4	Meramec	Interbedded Bioclastic Calcareous Siltstone	light gray color, thicker (cm) laminations (planar and inclined), hydrocarbon staining occurs along microfault in sample, stylolite's prominent, bioclasts prominent, calcareous (strong reaction to HCL), moderately sorted
Dewey-5	Meramec	Bioclastic Bioturbated Argillaceous Calcareous Siltstone	mottled dark gray color, lack of bedding preserved, bioturbated, bioclastic (increased shell content), increased mud/clay content (argillaceous), calcareous (strong reaction to HCL), moderately sorted

Canadian-1	Meramec	Calcareous Argillaceous Siltstone	dark gray-brown color, thinly laminated (planar), increased mud/clay content (argillaceous), calcareous (moderate reaction to HCL), very well sorted
Canadian-2	Meramec	Calcareous Argillaceous Siltstone	dark gray-brown color, thinly laminated (planar and inclined), coarse silt/very fine sand are concentrated along inclined laminations and mud/clay are concentrated along planar laminations, increased mud/clay content (argillaceous), calcareous (moderate reaction to HCL), very well sorted
Canadian-3	Meramec	Calcareous Siltstone	light gray color, no visible laminations (homogeneous), calcareous (strong reaction to HCL), very well sorted
Canadian-4	Meramec	Bioturbated Calcareous Siltstone	mottled dark gray color, lack of bedding preserved, heavily bioturbated, slightly argillaceous, calcareous (moderate to strong reaction to HCL), well sorted
Canadian-5	Meramec	Calcareous Argillaceous Siltstone	dark gray-black color, thinly laminated (poorly), few bioclasts visible, high mud/clay content (argillaceous), calcareous (moderate reaction to HCL), well sorted
S-15	Sycamore	Calcareous Siltstone	light gray color, very subtle thin laminations (planar), well-sorted, calcareous (strong reaction to HCL)
ES-1	Sycamore	Calcareous Siltstone	light tan-gray color, thinly laminated (planar), well-sorted, graded bedding, calcareous (strong reaction to HCL)

CNY-1	Caney	Fine Grained Sandstone	light yellow-brown color, well-sorted, less resistive, fine sand, quartz rich, laminated bedding, limonite rind (weathering product), non calcareous (no reaction to HCL)
PQ-01	Pryor Creek; "Ordnance Mbr"	Calcareous Bioclastic Siltstone	light gray color, thinly laminated (planar), well-sorted, subtle graded bedding (less frequent), calcareous (strong reaction to HCL), few shell and other bioclast fragments
PQ-04	Pryor Creek; "Lindsey Brdge Mbr"	Calcareous Siltstone	light gray color, thinly laminated, well-sorted, pyrite crystals, calcareous (strong reaction to HCL)
MRFD-01	Moorefield	Calcareous Shale	black color, thinly laminated (planar; mud and silt), calcareous (strong reaction to HCL), fissile and friable, well sorted
MRFD-02	Moorefield	Calcareous Very Fine Siltstone	dark gray color, calcareous (strong reaction to HCL), very well sorted
MRFD-03	Moorefield	Calcareous Siltstone	dark gray color, thinly laminated (planar; mud and silt), graded bedding, calcareous (strong reaction to HCL), well sorted
BTVL-01	Batesville	Medium Grained Sandstone	brown color (weathered) and yellow color (unweathered), cross-bedded, medium to fine sand, quartz rich, moderate-well sorted

Table 3: Summary of Thin Section Petrography

Sample_ID	Wentworth Grain Size Class	Roundness	Sorting	Porosity	Depositional Features	Petrographic Description
Dewey-1	silt	angular	very well	<1%	thin laminations (inclined, planar), graded bedding	P displays albite twinning (unstained), calcite is stained pink, muddy-carbonate cement (~30%), matrix supported
Dewey-2	silt	angular to subangular	very well	7%	thin laminations (bioturbated)	P displays albite twinning (unstained), calcite is stained pink, bioturbation structures disrupt laminated bedding and are filled with mixture of calcite and quartz grains, numerous grains stained with hydrocarbons
Dewey-3	silt	angular	well	<1%	graded bedding	pyrite grains concentrated along bedding planes (possible mineral placers?), few bioclastic shell fragments (<10%, stained pink due to calcite), matrix supported (~40%, orange-brown in xpl), inferred Qp grains might be Ls grains that are quartz-rich, P displays albite twinning and is not stained
Dewey-4	silt	angular	poorly to very poorly	<1%	graded bedding	large bioclasts (sponges, radiolarian, shells) and ooids (~30%, stained pink due to calcite content), Qm grains appear to have a coating along the edges, some grains have hydrocarbon staining, inferred Ls grains are quartz-rich with few carbonate lithologies
Dewey-5	silt	angular	moderately to well	<1%	graded bedding	large bioclast fragments (intact shells concave downward) in the upper fraction of the thin section (~10%), bioclasts stained pink due to calcite, bioclast content increases upwards (few small fractured bioclast grains present at base), inferred Ls are dominantly carbonate (dolostone/limestone) but some Ls grains quartz-rich, P grains display albite twin and are not stained

Canadian-1	silt	angular	very well	<1%	thin laminations, graded bedding	much of the matrix/probable pore space (~30%) is filled by black (hydrocarbon?), P displays albite twinning but is not stained, carbonate (Ls grains (dolostone/limestone), or calcite), graded bedding, spherical grains present (peloids?)
Canadian-2	silt	angular to subangular	well	<1%	thin laminations, graded bedding	P displays albite twinning (many grains are stained pink, some display excellent twinning but are not stained), a couple P grains present are larger in size: up to fine-upper <250 μ , carbonate content (possibly Ls grains (dolostone/limestone or calcite), bottom of thin section contains a graded bed that contains finer grained quartz rich fraction and transitions towards P-rich coarser grained fraction before terminating, large P grains are only seen in the lower bed in this thin section
Canadian-3	silt	angular	very well	<1%	grains aligned parallel to surface, no bedding/grading	P displays albite twinning but is not stained, hydrocarbon staining on a variety of grain types (appears to be black and splotchy), carbonate cement appears stained red (~40%), spherical radiolarian present (~15%)
Canadian-4	silt	subangular to subrounded	very well	<1%	thin laminations (lenticular)	lenticular lenses are made of muddy matrix (~50%) composed of platy clay minerals, down lapping surfaces onto thin laminations (low angle clinofolds: prograding), grains are oriented in similar manner with long axis parallel to prograding clinofolds, P grains have distinct albite twinning
Canadian-5	silt	angular	very well	<1%	thin laminations (lenticular)	lenticular lenses are made of muddy matrix (~50%) composed of platy clay minerals, Ls grain is larger in size (<150 μ) and appears to be a drop stone with condensed laminations beneath and sediment blanketing the top of the grain, carbonate grains (calcite) including some bioclasts make up (~10%)
S-15	silt	subangular to angular	very well	<1%	thin laminations	laminations marked by concentrations of Qm, carbonate cement (calcite, ~60%)

ES-1	silt	subangular to angular	very well	3%	thin laminations, graded bedding	carbonate cement (calcite, possibly some dolomite), matrix supported (~50%), carbonate looks to be stained
CNY-1	fine sand	subangular to angular	very well	25%	none; due to cut of thin section	Qch grains typically surround Qm grains, increased porosity
PQ-01	silt	angular	very well	<1%	thin laminations	Qm concentrated along thin laminations, contains some bioclasts (~10%), carbonate cement (calcite, ~35%)
PQ-04	silt	angular	very well	<1%	thin laminations	matrix supported, carbonate cement (calcite, ~50%)
MRFD-01	silt	angular to subangular	moderately to well	<1%	thin laminations	some Qm grains contain vacuoles, P is weakly stained orange and displays albite twinning, argillaceous/muddy matrix (~20%) fills between grains, Ls grains are mixture of quartz-rich and possibly mudstone, few larger grains (~250 μ) are Ls and appear to be drop stones
MRFD-02	silt	subangular to angular	very well	<1%	none; due to cut of thin section	P is stained pink-orange and appears to be altered (many grains are degraded and being replaced by calcite), few P grains display excellent albite twinning are not stained or degraded, a variety of grains are stained by hydrocarbons, sample is dominated by carbonate matrix (calcite, ~75%), calcite has likely replaced numerous P grains
MRFD-03	silt	angular	very well	<1%	thin laminations, graded bedding	P is stained pink-orange but is degraded (unable to find grains with twinning), bioclast fragments (~30%) comprised of calcite are oriented parallel to bedding, argillaceous-micritic matrix (40%). Hydrocarbon staining prominent.
BTVL-01	fine-medium sand	subangular to angular	moderately to poorly	40%	cross stratified	thin section is not stained, numerous grains have black stains on the surface (possibly hydrocarbons), grain supported, several Qm grains contain vacuoles, few accessory minerals (rutile, zircon), several pore spaces are stained pink-orange along the edges (potentially where a Feldspar was weathered).